

**Diurnal variation of
NO₃ over TMF**

C. M. Chen et al.

This discussion paper is/has been under review for the journal Atmospheric Chemistry and Physics (ACP). Please refer to the corresponding final paper in ACP if available.

Diurnal variation of midlatitudinal NO₃ column abundance over Table Mountain Facility, California

C. M. Chen^{1,*}, R. P. Cageao^{1,**}, L. Lawrence^{2,***}, J. Stutz², R. J. Salawitch^{1,****},
L. Jourdain^{1,*****}, Q. B. Li^{1,2}, and S. P. Sander¹

¹Jet Propulsion Laboratory, California Institute of Technology, Pasadena, California, USA

²University of California, Los Angeles, California, USA

* now at: Potsdam Institute for Climate Impact Research, Potsdam, Germany

** now at: NASA Langley Research Center, Hampton, Virginia, USA

*** now at: California Air Resources Board, Sacramento, California, USA

**** now at: University of Maryland, College Park, Maryland, USA

***** now at: Laboratoire de Physique et Chimie de l'Environnement et de l'Espace, Université d'Orléans/CNRS

Received: 22 June 2010 – Accepted: 30 July 2010 – Published: 26 August 2010

Correspondence to: C. M. Chen (claudine.chen+acp@googlemail.com)

Published by Copernicus Publications on behalf of the European Geosciences Union.

Title Page	
Abstract	Introduction
Conclusions	References
Tables	Figures
◀	▶
◀	▶
Back	Close
Full Screen / Esc	
Printer-friendly Version	
Interactive Discussion	



Abstract

The column abundance of NO_3 was measured over Table Mountain Facility, CA (34.4° N, 117.7° W) from May 2003 through September 2004, using lunar occultation near full moon with a grating spectrometer. The NO_3 column retrieval was performed with the differential optical absorption spectroscopy (DOAS) technique using both the 623 and 662 nm NO_3 absorption bands. Other spectral features such as Fraunhofer lines and absorption from water vapor and oxygen were removed using solar spectra obtained at different airmass factors. We observed a seasonal variation, with nocturnally averaged NO_3 columns between $5\text{--}7 \times 10^{13}$ molec cm^{-2} during October through March, and $5\text{--}22 \times 10^{13}$ molec cm^{-2} during April through September. A subset of the data, with diurnal variability vastly different from the temporal profile obtained from one-dimensional stratospheric model calculations, clearly has boundary layer contributions; this was confirmed by simultaneous long-path DOAS measurements. However, even the NO_3 columns that did follow the modeled time evolution were often much larger than modeled stratospheric partial columns constrained by realistic temperatures and ozone concentrations. This discrepancy is attributed to substantial tropospheric NO_3 in the free troposphere, which may have the same time dependence as stratospheric NO_3 .

1 Introduction

NO_3 plays a significant role in the chemistry of the stratosphere and troposphere. In the stratosphere, it influences the partitioning of active nitrogen species NO and NO_2 (NO_x), where NO_x is an important component in catalytic ozone loss cycles. The primary source of NO_3 is a reaction between NO_2 and O_3 (R1), and it is consumed by an additional reaction with NO_2 to form the reservoir species N_2O_5 (R2).



Diurnal variation of NO_3 over TMF

C. M. Chen et al.

Title Page

Abstract

Introduction

Conclusions

References

Tables

Figures

◀

▶

◀

▶

Back

Close

Full Screen / Esc

Printer-friendly Version

Interactive Discussion



**Diurnal variation of
NO₃ over TMF**

C. M. Chen et al.

Title Page

Abstract

Introduction

Conclusions

References

Tables

Figures

◀

▶

◀

▶

Back

Close

Full Screen / Esc

Printer-friendly Version

Interactive Discussion



The subsequent removal of N₂O₅ via a heterogeneous reaction with water to form nitric acid, also a reservoir species for NO_x but with longer lifetime, contributes to NO_x removal. The thermal decomposition of N₂O₅ is an additional significant source of NO₃ in the upper stratosphere. Since NO₃ photodissociates extremely rapidly at wavelengths less than about 640 nm, we observe significant concentrations only at night.

In the troposphere the same creation and destruction reactions occur, and there is also negligible NO₃ during sunlit hours except for extremely polluted urban settings (Geyer et al., 2003). In the boundary layer, NO₃ additionally is an important nighttime oxidant because it reacts rapidly with many biogenic hydrocarbons such as alkenes, aldehydes and terpenes (Atkinson, 1991; Wayne et al., 1991).

Interest in the role played by NO₃ in atmospheric chemistry increased significantly following the first reports of its detection in the stratosphere and troposphere by Noxon et al. (1978, 1980) and Platt et al. (1980). Since then, other measurements of atmospheric NO₃ column at low and midlatitudes at urban-influenced and remote ground-based sites have been made by using the Moon as a light source and employing differential optical absorption spectroscopy (DOAS) (Aliwell and Jones, 1996a,b, 1998; Lal et al., 1993; Renard et al., 2001; Solomon et al., 1989). Also, vertical concentration profiles of NO₃ have been inferred from ground-based measurements by observing NO₃ in the slant column during sunrise with direct lunar, zenith sky, and off-axis methods (Allan et al., 2002; Coe et al., 2002; Smith and Solomon, 1990; Smith et al., 1993; von Friedeburg et al., 2002; Weaver et al., 1996). As the solar terminator sweeps from the upper atmosphere down to the surface, photolysis progressively decreases the column of NO₃, leaving only the column that lies below the terminator altitude. Additionally, stratospheric profiles of NO₃ have been obtained from the SAGE III (Stratospheric Aerosol and Gas Experiment) and SCIAMACHY (SCanning Imaging Absorption spectrometer for Atmospheric Cartography) (Amekudzi et al., 2005) satellite instruments using lunar occultation, and the GOMOS (Global Ozone Monitoring by Occultation of Stars) (Hauchecorne et al., 2005; Marchand et al., 2004) satellite instrument using stellar occultation.

**Diurnal variation of
NO₃ over TMF**

C. M. Chen et al.

A number of measurements have confirmed the role of NO₃-N₂O₅ chemistry in the nocturnal boundary layer (Aldener et al., 2006; Allan et al., 2000; Ambrose et al., 2007; Ayers and Simpson, 2006; Brown et al., 2003, 2004; Carslaw et al., 1997a; Geyer et al., 2001; Geyer and Platt, 2002; Li et al., 2008; Matsumoto et al., 2006; Mihelcic et al., 1993; Nakayama et al., 2008; Smith et al., 1995; Stutz et al., 2004; Vrekoussis et al., 2007; Wang et al., 2006). Fewer have probed above the boundary layer, essentially those using LP-DOAS (Carslaw et al., 1997b), aircraft measurements (Brown et al., 2007a,b) and zenith sky measurements at sunrise (Allan et al., 2002; Coe et al., 2002; von Friedeburg et al., 2002). Due to this relative lack of measurements above the boundary layer, our quantitative understanding of the role of NO₃-N₂O₅ chemistry in the free and upper troposphere is incomplete.

Our focus is on the quantification of NO₃ in the free troposphere. We deduce time-resolved estimates of free tropospheric NO₃ using measurements of total column NO₃, observations of the boundary layer concentration of NO₃, with stratospheric columns provided by a model. Specifically, we present results of simultaneous measurements of NO₃ column by lunar occultation with the DOAS technique, and surface concentration of NO₃ using LP-DOAS, taken on evenings near full moon in August and September 2004 over Table Mountain Facility (TMF), California. Profiles of NO₃ found using a stratospheric model, shown to be consistent with SAGE III satellite lunar occultation measurements of NO₃, provided stratospheric partial columns with inputs from a climatology constructed from over 10 yr of lidar measurements at our measurement site. We also used global chemistry and transport model GEOS-Chem to characterize the time evolution and vertical distribution of NO₃ in the troposphere for various locations. The full dataset of NO₃ column measurements was taken from May 2003 through September 2004, and we characterized the magnitude and variability of column NO₃ at TMF, a location near Los Angeles influenced by clean and polluted air masses.

[Title Page](#)[Abstract](#)[Introduction](#)[Conclusions](#)[References](#)[Tables](#)[Figures](#)[I◀](#)[▶I](#)[◀](#)[▶](#)[Back](#)[Close](#)[Full Screen / Esc](#)[Printer-friendly Version](#)[Interactive Discussion](#)

2 Experiment description

2.1 Location and measurement frequency

We have acquired direct lunar occultation measurements of the NO₃ column at Table Mountain Facility (TMF), California (34.4° N, 117.7° W) at an altitude of 2280 m. TMF is in the San Gabriel Mountains north of the Los Angeles Basin and south of the Mojave Desert. Optimal measurements were acquired within the period two days before and two days after full moon. Full moon conditions offer the longest period of moonlit evening hours and the highest signal to noise due to the intensity of reflected sunlight with lunar phase angle opposition effect (Hapke et al., 1993). Observations from May 2003 through September 2004 consisted of three evenings for each full moon event, weather permitting, and resulted in 40 d of data.

2.2 Lunar occultation measurement

2.2.1 Instrument configuration

The experimental apparatus (Cageao et al., 2001) is shown in Fig. 1. Light was collected by a heliostat and directed into an off-axis telescope with 3× magnification. The 7-cm diameter collimated beam from the telescope was transmitted through a condensing lens, a shutter and order sorting filter (Schott GG-400 glass) to a 0.3 m focal length, f/4 imaging spectrometer (Acton 300i) with a 1200 g/mm blazed grating. A slit width of 150 μm was used, resulting in 0.4 nm (FWHM) spectral resolution. Wavelength calibration for the spectrometer was obtained by observing a neon Penray lamp mounted on the inside of the observatory dome. The shape and line width of these emission lines also provided the instrument lineshape function.

The spectrometer was equipped with a 1024×255, back-illuminated CCD detector temperature stabilized with circulating coolant. The pixel spacing of the CCD was 26 μm, which resulted in seven times oversampling of the instrument line width defined

Title Page

Abstract

Introduction

Conclusions

References

Tables

Figures

◀

▶

◀

▶

Back

Close

Full Screen / Esc

Printer-friendly Version

Interactive Discussion



**Diurnal variation of
NO₃ over TMF**

C. M. Chen et al.

Title Page

Abstract

Introduction

Conclusions

References

Tables

Figures

◀

▶

◀

▶

Back

Close

Full Screen / Esc

Printer-friendly Version

Interactive Discussion



by the entrance slit projected on the focal plane. For the initial observations, the CCD detector operated in imaging mode, with an integration time of three seconds at peak lunar intensity. The intensity of the moon decreases rapidly off full moon (50% decrease two days from full moon) and with increasing airmass, so the integration time was adjusted to maintain a constant CCD exposure level. Spectra, obtained between sunset and sunrise, were recorded every 10–20 min, yielding at least 30 column abundance values for each evening. In the more recent datasets, June, August, and September of 2004, the collection frequency was increased to a spectrum every minute to improve the time resolution. This increased the number of column measurements to over 400 per night.

To improve the signal-to-noise ratio, five scans were averaged to obtain a single archived spectrum. There were similar integration times among the five scans averaged, but total integration time could differ when comparing averaged data on and off full moon. For measurements in June, August, and September of 2004, the detector was run in a mode that acquired 29 spectra which were summed for each archived spectrum, with a total integration time of 7.25 s at peak lunar intensity. All spectra were dark-corrected, but not flat-fielded, since pixel-to-pixel variability canceled with comparison to the reference spectrum, as described below.

2.2.2 Spectral analysis

Remote and in situ sensing of atmospheric NO₃ make use of the strong vibrational bands at 662 and 623 nm which are assigned to the (0,0) and (1,0) bands, respectively, of the ν_1 symmetric stretch in the $A^2E' \leftarrow X^2A_2'$ electronic transition (Ramsay, 1962). High resolution laboratory spectroscopy studies have shown these bands are diffuse with cross sections that are weakly dependent on temperature (Cantrell et al., 1987; Ravishankara and Mauldin, 1986; Sander, 1986; Yokelson et al., 1994) decreasing by 22% over the range of atmospheric temperatures from 220 to 298 K. For ground-based remote sensing studies of NO₃, spectroscopic interferences with these bands include the O₂ gamma band at 628.8 nm, and a weak water vapor band in the 640–665 nm

spectral region. There are also absorption bands in this spectral range for O_4 and NO_2 , but the contribution from these bands was negligible at Table Mountain. O_4 scales with the square of O_2 concentration, and therefore exists primarily at the surface. NO_2 has very weak lines in this spectral range that are lost in the noise for this measurement.

5 The spectrometer dispersion and grating position were selected to give a spectral bandpass of 617–674 nm. In this spectral interval we recorded and analyzed both the 623 and 662 nm absorption bands of NO_3 . The spectra were analyzed using the differential optical absorption spectroscopy (DOAS) approach (Platt and Stutz, 2008) with the spectral analysis and deconvolution program, MFC (Stutz and Platt, 1996).

10 The principle of DOAS is to use only the high-frequency components of the spectrum to determine the quantity of an optically absorbing atmospheric component. The effect of the DOAS processing steps on the data is shown in Fig. 2. First, the slowly varying low frequency component of the background, from sources such as Rayleigh and Mie scattering effects and solar flux spectral variations, was removed numerically from the lunar occultation spectra. This was done by dividing the raw data with a smoothed
15 version of the same data. Shown in Fig. 2b is the logarithm of this ratio, making the spectrum proportional to column abundance and molecular absorption cross section. The reflected solar Fraunhofer lines that dominate the raw spectra were then removed using solar reference spectra. The high-pass filtered lunar spectrum was divided by
20 a high-pass filtered solar reference spectrum after aligning the spectra in wavelength with a nonlinear fit with stretch. The resulting spectrum was fit by least squares to high-pass filtered reference spectra of NO_3 , H_2O , and O_2 (Fig. 2c).

25 The slant NO_3 column abundances calculated from the fit were converted to vertical column abundances by dividing by the airmass, a factor that describes the amount of air seen through a slant path in the atmosphere compared to a view directly overhead. The airmass was determined from the reciprocal of the cosine of the lunar zenith angle (a valid approximation for angles up to 80°) with an additional small correction for refraction.

**Diurnal variation of
 NO_3 over TMF**

C. M. Chen et al.

Title Page

Abstract

Introduction

Conclusions

References

Tables

Figures

I◀

▶I

◀

▶

Back

Close

Full Screen / Esc

Printer-friendly Version

Interactive Discussion



**Diurnal variation of
NO₃ over TMF**

C. M. Chen et al.

[Title Page](#)[Abstract](#)[Introduction](#)[Conclusions](#)[References](#)[Tables](#)[Figures](#)[◀](#)[▶](#)[◀](#)[▶](#)[Back](#)[Close](#)[Full Screen / Esc](#)[Printer-friendly Version](#)[Interactive Discussion](#)

To obtain the reference spectra for the solar features, we recorded direct solar spectra with two ground glass diffuser plates in the light path between the heliostat and telescope. The primary purpose of the diffuser plates was to average the observed radiance over the entire solar disk. Without the plates, only a small fraction of the solar disk was imaged onto the spectrometer slit. The solar spectral features in the non-diffuse spectra differed from those in the lunar spectra. The diffuser plates also helped to attenuate the solar beam, although additional neutral density filtering was used to avoid detector saturation.

Solar reference spectra were acquired over a day for the airmass range 1–7 (SZA 34–81°). New solar reference spectra were taken once a month during the time of the full moon datasets to account for small changes in instrument alignment. In addition to solar lines, these spectra contained terrestrial water vapor and O₂ features with optical depths that were proportional to the airmass. The solar reference spectrum used in the processing for a particular lunar spectrum had an airmass within ±0.5 of the airmass of the lunar data, thereby removing much of the water and O₂ column prior to additional processing. To account for the remaining and variable water vapor and O₂ signal, ratios of solar spectra at different airmasses provided empirical water and O₂ reference spectra. Since there is little overlap of these two spectral features, the O₂ and water features were individually isolated and used as empirical spectral references. The low spectral resolution of measurement does not resolve individual lines for water and O₂, and therefore has little sensitivity to pressure broadening.

The NO₃ reference spectra used were obtained from laboratory absorption cross section studies of NO₃ and have been measured over the temperature range relevant to the troposphere and stratosphere (Cantrell et al., 1987; Ravishankara and Mauldin, 1986; Ravishankara and Wine, 1983; Sander, 1986; Yokelson et al., 1994). The cross sections of Sander (1986) and Yokelson et al. (1994) are in excellent agreement over the range of overlap of temperature. Both studies observed a significant decrease in NO₃ cross sections at the peaks of the 662 and 623 nm bands with decreasing temperature. In contrast, the results of Cantrell et al. (1987) showed no dependence of cross

section with temperature and are assumed to be incorrect. The results of Ravishankara and Mauldin (1986) disagree significantly with those of Yokelson et al. (1994) from the same group, and are assumed to be superseded by the latter. Although the temperature at the peak of the stratospheric NO₃ concentration profile at 40 km is roughly 260 K, the average temperature weighted by the model-predicted NO₃ concentration profile in the stratosphere is closer to 240 K. We have used the spectrum of Yokelson et al. (1994) at 240 K for the column retrievals presented here. Solomon et al. (1989) also used a reference temperature of 240 K, while Aliwell and Jones (1998) used 260 K.

2.2.3 Measurement uncertainty

The overall uncertainty for our measurement of total column NO₃ is approximately 17% RMS. The most important contributions to this uncertainty are systematic errors in cross section, and photon noise. The stated uncertainty in the NO₃ cross section is ±10% (Yokelson et al., 1994), excluding the errors associated with the temperature dependence of the cross sections. Our estimate of total column NO₃ assumes that the absorption is dominated by stratospheric contributions. There is a ±6% error associated with the use of a single cross section at a temperature of 240 K, if the temperature of the column actually varies between 220 and 260 K. If there are contributions from tropospheric NO₃, the retrieved columns are a lower limit since the cross section of the band peak at 662 nm for 298 K is 17% less than for 240 K. Photon noise in the system contributes an estimated 13% to the uncertainty. The detection limit for the NO₃ slant column abundance is 2×10^{12} molec cm⁻². The signal to noise ratio was >5 for most of the evening (during the steady state growth period); this ratio was larger for measurements through larger airmasses or larger NO₃ column amounts.

2.3 Long-path DOAS instrument

Horizontal column average measurements were made at TMF for August and September 2004 using a long-path differential optical absorption spectrometer (LP-DOAS).

Diurnal variation of NO₃ over TMF

C. M. Chen et al.

Title Page

Abstract

Introduction

Conclusions

References

Tables

Figures

◀

▶

◀

▶

Back

Close

Full Screen / Esc

Printer-friendly Version

Interactive Discussion



**Diurnal variation of
NO₃ over TMF**

C. M. Chen et al.

Title Page

Abstract

Introduction

Conclusions

References

Tables

Figures

◀

▶

◀

▶

Back

Close

Full Screen / Esc

Printer-friendly Version

Interactive Discussion



LP-DOAS is an active remote sensing technique that gives exceptionally low detection limits by averaging over a long (several kilometers) pathlength. Light from a broad-spectrum 500W Xe arc lamp was collimated through a Newtonian telescope and broadcast to an array of corner-cube retroreflectors mounted on a radio tower located on the Blue Ridge in the Angeles National Forest. The distance between the instrument and the retroreflector array was approximately 3.4 km. Light incident on the retroreflector array traveled back through the atmosphere, was collected by the same telescope and transmitted through a fiber-optic cable to the spectrometer and detector. The difference in altitude between the LP-DOAS instrument and the tower-mounted retroreflector array was 298 m. A detailed description of the LP-DOAS instrument and the NO₃ analysis employed here is given in (Geyer et al., 1999). The measurement uncertainty of the LP-DOAS is dominated by the error in the absorption cross-section of NO₃, which is ±10% (Yokelson et al., 1994) as previously noted.

3 Model descriptions

3.1 1-D stratospheric model

A one-dimensional, photochemical steady state model of the stratosphere (Osterman et al., 1997) was run using TMF climatological profiles of temperature and O₃ as inputs, and the modeled NO₃ column abundances were compared to the TMF column measurements. The model calculates diurnally varying species concentrations, assuming each species reaches a balance between production and loss over 24 h for a given temperature and pressure profile and latitude. JPL 2006 cross sections and quantum yields were used to determine photolysis J values, and JPL 2006 kinetic rate constants were used for reaction rates (Sander et al., 2006, 2003). Chemical inputs are profiles of O₃, H₂O, CH₄, NO_y, Cl_y, CO, H₂, C₂H₆, Br_y, and aerosol parameters based on a climatology derived from NASA satellite and balloon observations (e.g., Yang et al., 2006), as detailed in Table 1.

Additionally, SAGE III satellite measurements of O_3 in the stratosphere were used to verify the consistency between the 1-D stratospheric model and SAGE III measurements of NO_3 , testing the current understanding of stratospheric NO_3 chemistry (described in Appendix A). Analysis of the sensitivity of modeled NO_3 column to input parameters and to uncertainties of reaction rates were also conducted and are described in Appendix B.

3.1.1 Table Mountain Facility lidar climatology

Temperature and ozone profiles have been measured at TMF by lidar since 1988 and offer a unique opportunity to compare our measurements with a model with realistic constraints. Temperature profiles were measured between 30–80 km and ozone profiles between 15–50 km, both with 300 m vertical resolution since September 1994 and with 600 m vertical resolution beforehand. Three cases were run using these data: climatological monthly mean values and variability over the 10 yr period 1988–1997 (data extracted from the published contour plots) (Leblanc and McDerimid, 2000; Leblanc et al., 1998), and monthly mean profiles for 2003 and for 2004 provided by Leblanc (2005). Temperature and ozone profiles are sufficient for estimating the NO_3 column since NO_3 is primarily determined by these two quantities, as verified from a sensitivity study described in Appendix B1.

The change in NO_3 column at the extremes of variability was probed by running the model with both temperature and ozone variability added or subtracted from the climatological temperature and ozone profiles. The uncertainty in the climatological temperature measurements are 0.6 K at the middle of the altitude range, 8 K at 30 km, and <4 K at 80 km. The uncertainty of the climatological ozone measurements are a few percent at the peak of the ozone, 10–15% at 15 km, and more than 40% above 45 km. The uncertainty in ozone for the 2003 and 2004 monthly mean profiles was a minimum at 6% at the ozone peak, increasing in error above and below this altitude to 10% at 18 km and 42 km. The uncertainty in temperature for the 2003 and 2004 monthly mean profiles varied between 0.5 and 1.3 K over 13–60 km.

Diurnal variation of NO_3 over TMF

C. M. Chen et al.

Title Page

Abstract

Introduction

Conclusions

References

Tables

Figures

◀

▶

◀

▶

Back

Close

Full Screen / Esc

Printer-friendly Version

Interactive Discussion



**Diurnal variation of
NO₃ over TMF**

C. M. Chen et al.

[Title Page](#)[Abstract](#)[Introduction](#)[Conclusions](#)[References](#)[Tables](#)[Figures](#)[◀](#)[▶](#)[◀](#)[▶](#)[Back](#)[Close](#)[Full Screen / Esc](#)[Printer-friendly Version](#)[Interactive Discussion](#)

The gaps in the ozone and temperature profiles were filled with the climatology from (1) the Upper Atmosphere Research Satellite (UARS) Reference Atmosphere Project (URAP) (Remedios et al., 2007; Wang et al., 1999; Randel et al., 1999), and then (2) a climatology dataset based on ozone data from Dütsch (1974) and ozone and temperature from the Middle Atmosphere Program (Barnett and Corney, 1985; Keating and Young, 1985), with adjustments to the ozone climatology based on in situ ozone measurements in the upper troposphere and lower stratosphere from many field programs. URAP is a compilation of global data from the CLAES, HALOE, HRDI, MLS and ISAMS instruments on the UARS satellite taken from April 1992 through seven years, processed into zonal monthly means with standard deviation. Two types of data were provided: “baseline” data obtained from April 1992 to March 1993, and “extended” datasets averaged over 7 yr. We used extended data where available. The ozone data used were from the extended time range, and the temperature data from the baseline time frame. We also used profiles of H₂O (extended), CH₄ (extended), and N₂O (baseline) from URAP. N₂O was used as a tracer to estimate model inputs for NO_y, Cl_y, and Br_y using well established tracer relations (e.g., Yang et al. (2006) and references therein).

Static profiles for CO and C₂H₆ from MkIV measurements (Toon, 1991; Sen et al., 1998), and a H₂ profile based on measurements in the stratosphere (Abbas et al., 1996; Dessler et al., 1994; Rockmann et al., 2003) were used for all months. Vertical profiles of sulfate aerosol surface area were based on zonal monthly mean measurements by SAGE II (Thomason et al., 1997) updated to include data acquired during the time of our NO₃ measurements.

3.2 GEOS-Chem tropospheric model

We use the GEOS-Chem global 3-D tropospheric chemistry and transport model (Bey et al., 2001; Park et al., 2004; Wu et al., 2007) to explore the spatial and temporal variability of NO₃ in the troposphere for a few days in August and September 2004, coinciding with our acquisition dates. The GEOS-Chem model (version

7.02.04, <http://acmg.seas.harvard.edu/geos/>) is driven by the assimilated meteorological GEOS-4 data from NASA Global Modeling and Assimilation Office (GMAO) with 6-h temporal resolution (3-h for surface variables and mixing depths) and a horizontal resolution of $1 \times 1.25^\circ$ with 55 layers in the vertical. The horizontal resolution of the GEOS-4 wind fields has been degraded to $2 \times 2.5^\circ$ for input into GEOS-Chem.

4 Results and discussion

4.1 Experimental results

As seen in model calculations in Fig. 3, the diurnal variation of stratospheric NO_3 can be characterized by four phases: daytime photolysis (negligible NO_3), sunset build-up (a rapid rise in NO_3 column), nocturnal steady state (a nearly linear, slow rise in NO_3 column), and sunrise destruction (rapid decrease in NO_3 column). These four stages were also observed in our measurements, except for some variations during the nocturnal steady state stage. Time series that monotonically increase, which occurs almost linearly during the steady state phase, are labeled as “model-like behavior” as seen in our measurements from September 2004 (Fig. 3b); this label does not necessarily mean that these data are purely stratospheric in origin. The remaining data are described as “non-modeled behavior”, and displayed a wide variety of different temporal behavior with variability ranging from one to several hours, as seen in our measurements from August 2004 (Fig. 3a).

For purposes of comparison, each night of data was reduced to a time-averaged mean column and a standard deviation over the steady state phase, which was taken to be two hours after sunset up to roughly 30 min before sunrise. An annual plot of all the mean columns, with $2\text{-}\sigma$ standard deviations as error bars, is shown in Fig. 4. For 26 of the 40 d of analyzed data, the NO_3 columns followed model-like behavior (open symbols in Fig. 4). Within this subset of data a seasonal variation was observed, more clearly shown in Fig. 5. The NO_3 mean column averaged over summer

Diurnal variation of NO_3 over TMF

C. M. Chen et al.

Title Page

Abstract

Introduction

Conclusions

References

Tables

Figures

◀

▶

◀

▶

Back

Close

Full Screen / Esc

Printer-friendly Version

Interactive Discussion



months (April through September) was 7.5×10^{13} molec cm⁻². The column averaged over winter months (October through March) was 5.5×10^{13} molec cm⁻², as summarized in Table 2; cloudy conditions limited the amount of data that could be acquired during winter and none was possible in 2003. We attribute the larger summertime values to a warmer atmosphere (both in the troposphere and stratosphere), which drives the thermal decomposition of N₂O₅ to form NO₂ and NO₃. In the 14 remaining cases with non-modeled behavior (closed symbols in Fig. 4), which occurred from May to early October, the range of mean columns was $6\text{--}22 \times 10^{13}$ molec cm⁻² and the range of standard deviations was $1\text{--}5 \times 10^{13}$ molec cm⁻². The low end of the range of standard deviations occurred for cases with relatively flat but decreasing temporal profiles, while the high end of the range was characterized by large oscillations in the NO₃ column.

The large oscillations in total column NO₃ that occurred over an evening did not originate from the stratosphere, since the primary source of variability in the stratosphere is from planetary waves, which have time scales longer than one day (Salby, 1984; Wu and Waters, 1996). Instead these variations are likely to arise from the troposphere. However, the complexity of mountain topography complicates the determination of the origin of the tropospheric air at TMF using traditional back trajectory methods. Depending on the movement of the air masses, we observed from a range of sources as diverse as desert air to polluted urban air and air from aloft due to mountain subsidence and drainage flow.

Model results by Lu and Turco (Lu and Turco, 1995, 1996; Lu et al., 2003) of the Los Angeles basin air flow give an idea of seasonal behavior during quiescent conditions. Their Surface Meteorology and Ozone Generation (SMOG) model calculates winds and tracer transport in the Los Angeles basin and surrounding mountain areas. Land warming by solar radiation propels onshore winds and upslope mountain flows during the day, with stronger winds in summer than winter. In the summer evenings, there are generally downslope flows from the mountains, and disorganized winds in the basin. Winter evenings have a stronger offshore component from radiative cooling of

**Diurnal variation of
NO₃ over TMF**

C. M. Chen et al.

Title Page

Abstract

Introduction

Conclusions

References

Tables

Figures

◀

▶

◀

▶

Back

Close

Full Screen / Esc

Printer-friendly Version

Interactive Discussion



mountaintops and subsidence, driving the air towards the lower pressure off the coast. This suggests that daytime urban air is transported toward the mountains and over the passes year-round, but winter evenings are more efficient at flushing urban air from the mountains to the coast.

5 The two observed regimes for total column NO_3 , model-like and non-modeled behavior, were consistent with the Lu and Turco analysis of local air flow. Between mid-October and April, when only model-like behavior was observed, there was little evidence for tropospheric contribution to the total column NO_3 . In the summer, the daytime onshore component coupled with weakly organized evening flow would often
10 lead to urban air being advected to the TMF site, resulting in large variations in detected NO_3 . A signature of urban influence on column NO_3 was observed for 14 out of 31 d, for data collected between mid-April and mid-October in 2003 and 2004.

In Fig. 5, our model-like behavior data are shown compared to other measured column measurements using lunar occultation with grating spectrometers, from Solomon et al. (1989) and Aliwell and Jones (1996b). Data from Solomon et al. (1989) were
15 taken from Fig. 10 of their paper and reduced by 18% to account for the updated NO_3 cross section of Yokelson et al. (1994) at 240 K, which was not available when the paper was published. The result of Aliwell and Jones (1996b) and our data are in good agreement. While some of our data and that of Solomon et al. (1989) have overlapping error bars, the majority of their data is roughly $1\text{--}2 \times 10^{13}$ molec cm^{-2} below the
20 TMF columns. Solomon et al. (1989) confirmed most of their data was primarily stratospheric NO_3 by analyzing the dependence of the NO_3 slant column on the lunar zenith angle (LZA) near the horizon ($\text{LZA} > 80^\circ$) (Solomon et al., 1989). A tropospheric NO_3 signal would grow much faster than the stratospheric NO_3 at high lunar zenith angles from slant path increases. We were not able to use this method to determine the tropospheric contribution because of pointing system view angles limited to less than 80° .
25

Surface concentration measurements of NO_3 were made with the UCLA LP-DOAS instrument during the August and September 2004 measurement periods. The results are shown along with the NO_3 column amounts measured by lunar occultation in Fig. 6.

Diurnal variation of NO_3 over TMF

C. M. Chen et al.

Title Page

Abstract

Introduction

Conclusions

References

Tables

Figures

◀

▶

◀

▶

Back

Close

Full Screen / Esc

Printer-friendly Version

Interactive Discussion



**Diurnal variation of
NO₃ over TMF**

C. M. Chen et al.

[Title Page](#)[Abstract](#)[Introduction](#)[Conclusions](#)[References](#)[Tables](#)[Figures](#)[◀](#)[▶](#)[◀](#)[▶](#)[Back](#)[Close](#)[Full Screen / Esc](#)[Printer-friendly Version](#)[Interactive Discussion](#)

As shown in the figure, the short time-scale features in the 29–31 August LP-DOAS data are reproduced in the column data, implying a large boundary layer contribution to the column on those days. Some features seen in the column measurements were not present in the surface concentrations, which could be due to changing thickness of the polluted layer.

In contrast, data from 27–29 September 2004 had a much smaller contribution from the boundary layer. The LP-DOAS instrument confirmed that there were low NO₃ concentrations at the surface, as show in Fig. 6. This period coincided with a Santa Ana wind event, characterized by a northerly downslope flow that advected dry desert air mixed with air from aloft over the measurement site. This circulation is driven by a high pressure system centered north of Southern California. This flow of air from the north over the mountains and through the passes to the LA basin drives wind speeds of 46 km/h and gusts in excess of 90 km/h, carrying urban pollution offshore and away from Table Mountain Facility. Air quality measurements of surface NO₂, CO, and O₃ from Air Quality Management District (AQMD) stations (California Air Resources Board, 2007) in Victorville (14306 Park Avenue), Azusa, downtown Los Angeles (North Main Street), and West Los Angeles (Westchester Parkway), positioned progressively from the desert in Victorville towards the ocean, verifies that low concentrations of surface urban pollutants were found in the Mojave Desert and into Los Angeles County, and that the diurnal cycle for these chemicals was disrupted for this time period (see Fig. 7).

4.2 Model results

4.2.1 Stratospheric model

Model results using averaged TMF temperatures over three different time periods are shown in Fig. 4: monthly averages from 2003, from 2004, and over a ten year period, 1988–1997. All three TMF model results exhibited a seasonal variability with higher values during the summer. Results from 2003 followed those of the ten-year average, with November through January having the lowest values of the year, and the highest

values in April and May. Results from 2004 deviated from the other runs with larger modeled columns for January that decreased to climatological values from March onwards. The TMF seasonal averages for total column NO_3 are listed in Table 2.

4.2.2 Tropospheric model

From the results of the GEOS-Chem 3-D chemical transport model, we investigated the expected range of tropospheric NO_3 column abundances for specific geographic regions. GEOS-Chem could not be used for quantitative comparisons with TMF observations since the grid size is too large to resolve the local meteorology and the detailed transport of pollution from the L.A. Basin. In order to understand the range of the expected NO_3 variability from the model, column abundances are compared for three different locations: TMF (mountainous region with nearby urban pollution sources, 33–35° N, 241.25–243.75° E), Western Colorado (northern midlatitude mountain area, 37–41° N, 251.25–253.75° E), and the Northern Midlatitude Pacific Ocean (no urban sources or orographic influences, 29–45° N, 178.75–228.75° E). In addition, we calculate the NO_3 column for the northern midlatitude zonal mean (29–45° N). The regions were compared for six evenings that coincide with data collection (the evenings of 28–30 August 2004 and 27–29 September 2004). Total columns as well as the partial columns from the boundary layer and free troposphere were calculated.

The boundary layer defined by the model for each time step was not used since the boundary layer is shallower during night time and does not reflect the pollution that was distributed throughout the boundary layer in the daytime. Instead, a column was constructed by setting the threshold to the maximum altitude of the top of the boundary layer for that day. This column is labeled as the “maximum boundary layer”, with the difference of the total with this quantity labeled as the “minimum free troposphere”.

The time evolution of tropospheric NO_3 , shown in Figs. 8 and 9, varied over the different regions but in most cases there was a sawtooth pattern not unlike that for the stratosphere: daytime photolysis with negligible NO_3 , a nearly linear rise in NO_3 column over the evening followed by a rapid decrease in NO_3 column at sunrise. The

Diurnal variation of NO_3 over TMF

C. M. Chen et al.

Title Page

Abstract

Introduction

Conclusions

References

Tables

Figures

◀

▶

◀

▶

Back

Close

Full Screen / Esc

Printer-friendly Version

Interactive Discussion



maximum boundary layer column tended to mimic the total column shape, but for all cases the minimum free tropospheric column consistently had the sawtooth pattern.

The diurnal averages, calculated with the same method as with the measurements, are summarized in Table 3. The model grid cell over Los Angeles has large tropospheric NO_3 columns from anthropogenic NO_x with roughly $20\text{--}70 \times 10^{13}$ molec cm^{-2} , while the data at a midlatitude mountainous region (Western Colorado) and without nearby urban sources (Northern Midlatitude Pacific) had significantly smaller tropospheric columns ($4\text{--}5 \times 10^{13}$ molec cm^{-2}). The minimum free tropospheric column was at its lowest over the mountain region, (1×10^{13} molec cm^{-2}). The midlatitude zonal mean value is 6×10^{13} molec cm^{-2} . These values are consistent with the difference between our TMF measurements of total column NO_3 and model amounts of stratospheric partial column NO_3 . As discussed below, this suggests that there is NO_3 in the free troposphere that can reside for days in substantial concentrations, indistinguishable from stratospheric NO_3 based solely on the time evolution (diurnal variation) of the measured signal.

4.3 Model and measurement comparison

The measured NO_3 columns along with results from 1-D stratospheric model constrained by measured temperatures and ozone concentrations from TMF showed a seasonal trend with higher NO_3 in the summer months. Measurements and model results from January–March 2004 were consistent within error bars as seen in Fig. 4, even duplicating the decrease in mean NO_3 column over these months not seen in the other model results. However, as seen in Table 2, the measured data are consistently larger than the modeled data by over 2×10^{13} molec cm^{-2} for both summer and winter averages. This suggests that there is significant NO_3 in the troposphere; the stratospheric model correlated well with measured stratospheric NO_3 columns from SAGE III, as discussed in Appendix A, therefore we believe the model is reliable.

While it is clear that our NO_3 columns exhibiting non-modeled behavior has contributions from the boundary layer, even days with established low surface NO_3

Diurnal variation of NO_3 over TMF

C. M. Chen et al.

Title Page

Abstract

Introduction

Conclusions

References

Tables

Figures

◀

▶

◀

▶

Back

Close

Full Screen / Esc

Printer-friendly Version

Interactive Discussion



concentrations, such as 27–30 September 2004 (Fig. 3b), had mean columns of NO_3 that were on average $2 \times 10^{13} \text{ molec cm}^{-2}$ more than the model amount. Low levels of NO_3 were detected by LP-DOAS in September, but the measured columns were still on average $2 \times 10^{13} \text{ molec cm}^{-2}$ greater than the modeled column, which is more NO_3 than a uniform troposphere with 3 ppt of NO_3 , the detection limit of the instrument. Other measurements have determined there can be significantly larger concentrations of NO_3 above the surface in the upper boundary layer and lower free troposphere, using zenith sky measurements at sunrise compared to surface DOAS measurements (Allan et al., 2002). GEOS-Chem results for the northern midlatitude band (29–45° N) for the six days in August and September 2004 highlighted in this study found that the average minimum free tropospheric column was $6 \times 10^{13} \text{ molec cm}^{-2}$ while the average maximum boundary layer column was $3 \times 10^{13} \text{ molec cm}^{-2}$. For this case, significant NO_3 existed in the free troposphere with smoothly varying diurnal variation that is indistinguishable from modeled stratospheric NO_3 diurnal variation. This result indicates there is a sizable contribution to the column of NO_3 from the troposphere above the boundary layer. Brown et al. (2007a) reached similar conclusions based on aircraft measurements over the east coast of the United States.

5 Conclusions

We have measured the diurnal variation of the NO_3 column over Table Mountain Facility, California (34.4° N, 117.7° W), using ground-based visible absorption spectroscopy of moonlight. We observed two sets of behavior during the steady state phase of the evening: one described as “model-like behavior” followed the expected slow linear increase (mean columns of $5\text{--}9 \times 10^{13} \text{ molec cm}^{-2}$ for 26 out of 40 d), and the other, called “non-modeled behavior”, showed large departures from model behavior, often correlated with large mean NO_3 columns ($6\text{--}22 \times 10^{13} \text{ molec cm}^{-2}$ over 14 out of 40 d) and large standard deviations (up to $5 \times 10^{13} \text{ molec cm}^{-2}$), mostly during May through early October. The changes in NO_3 column seen in the non-modeled data are not likely

Diurnal variation of NO_3 over TMF

C. M. Chen et al.

[Title Page](#)[Abstract](#)[Introduction](#)[Conclusions](#)[References](#)[Tables](#)[Figures](#)[I◀](#)[▶I](#)[◀](#)[▶](#)[Back](#)[Close](#)[Full Screen / Esc](#)[Printer-friendly Version](#)[Interactive Discussion](#)

due to variability in the stratosphere and are attributed to boundary layer sources.

Comparison to results from a 1-D photochemical model with temperature and ozone profiles taken from onsite lidar instruments showed that for the most part we measured more NO_3 than found using the model. The model compares well with stratospheric column NO_3 reported by SAGE III. These comparisons suggest significant contributions to total column NO_3 from the free troposphere at all times, with the tropospheric contribution exhibiting a diurnal pattern similar to the stratospheric column. This is supported by simultaneous surface measurements with LP-DOAS in September 2004, and results from the global tropospheric chemical and transport model, GEOS-Chem.

Appendix A

The SAGE III (Meteor-3M) instrument (SAGE III ATBD, 2002) retrieved NO_3 concentration profiles from 20–60 km and O_3 concentration profiles from 15–50 km by satellite lunar occultation at moonset or moonrise. The retrieval process used temperature and pressure profiles from meteorological data from the National Centers for Environmental Prediction (NCEP) (Kalnay et al., 1996). These NCEP temperature and pressure profiles along with the SAGE III retrieved O_3 profiles were used as inputs for the stratospheric model and the resulting modeled NO_3 columns were compared with SAGE III NO_3 measurements. Available data spans from May 2002 to October 2005 (the mission was terminated March 2006), and 1184 data points from the latitude band between -70 and 70° were used; local times of the measurements were between 22:00–02:00 LT.

The 1-D stratospheric model described in the paper was run with inputs from SAGE III lunar O_3 measurements as well as the temperature and pressure data from NCEP reanalysis used in the SAGE III retrievals. The O_3 profile below 15 km and above 50 km was filled with a climatology based on Dütsch and the Middle Atmosphere Project, described in the model description in the body of the paper; this has little impact on the scientific interpretation of our results, since the altitude range of interest for NO_3

Diurnal variation of NO_3 over TMF

C. M. Chen et al.

Title Page

Abstract

Introduction

Conclusions

References

Tables

Figures

◀

▶

◀

▶

Back

Close

Full Screen / Esc

Printer-friendly Version

Interactive Discussion



is covered by the SAGE III measurements. The rest of the chemical inputs were the same as described for the TMF model runs.

The NO₃ profiles were integrated over the 18–60 km altitude range to determine a stratospheric partial NO₃ column comparable to the one calculated from SAGE III data. These columns were further reduced to a mean column and standard deviation calculated over the nocturnal steady state period, as done with our measurements.

The modeled stratospheric NO₃ columns are plotted against the values derived from integration of the SAGE III NO₃ vertical profiles in Fig. 10. The bulk of the data points cluster along the one-to-one line. Since both sets of data have significant uncertainties, we used a linear fit that considered both x and y errors (the details are described in Wang et al., 2008), rather than a standard linear fit that considers only errors in y . The uncertainty in the modeled NO₃ column due to uncertainties in input temperature and O₃ profiles was estimated to be 0.7×10^{13} molec cm⁻², and uncertainty in the measured NO₃ column derived from the quoted uncertainties in the SAGE III NO₃ retrieved profiles was 0.2×10^{13} molec cm⁻². This resulted in a linear fit with a slope of 0.92 ± 0.02 and an intercept of $0.42 \pm 0.5 \times 10^{13}$ molec cm⁻², with a reduced Chi squared, χ_{red}^2 , of 4.3. The reduced Chi squared is the χ^2 statistic normalized by the degrees of freedom, with a value of one indicative of a good fit (residual of fit and data is same order as errors), much less than one an indication of overestimated errors, and much greater than one of underestimated errors. From these fit results we assert that the modeled stratospheric NO₃ columns are consistent with the SAGE III measured columns.

Appendix B

B1 Sensitivity Study of modeled NO₃ on input parameters in 1-D stratospheric model

We conducted a sensitivity study of the 1-D stratospheric model to determine to which input parameters the NO₃ column was most sensitive. Changes of $\pm 5\%$ concentration or ± 5 K were applied to the entire vertical profile of an individual input parameter. These

Diurnal variation of NO₃ over TMF

C. M. Chen et al.

Title Page

Abstract

Introduction

Conclusions

References

Tables

Figures

◀

▶

◀

▶

Back

Close

Full Screen / Esc

Printer-friendly Version

Interactive Discussion



changes were applied to atmospheric profiles using the URAP climatology for all twelve months. Other chemical profiles not provided by URAP used the same sources as described for the TMF model runs.

We found that out of the various input parameters to the 1-D model, the NO_3 column is most sensitive to temperature and O_3 . An increase or decrease of temperature by 5 K in the model resulted in change in the mean NO_3 column by 36 or -25% , respectively. A linear response was observed below 30 km; from 30–45 km a strongly nonlinear response was observed. A change of $\pm 5\%$ in the ozone concentration resulted in a change in the mean NO_3 column by $\pm 5\%$, with no altitude dependence in the sensitivity from 18–50 km. This directly proportional, linear relationship between NO_3 and ozone concentration occurs when NO_3 concentration is in steady state. NO_y also had a small effect, with the $\pm 5\%$ change in NO_y concentration resulting in a $\pm 1\%$ change in the NO_3 column. The effect on NO_3 from changes in the input concentration of other chemicals was negligible. These sensitivity coefficients are summarized in Table 4.

B2 Error propagation of reaction rates to NO_3 columns

Sensitivity of the NO_3 column to the errors in the rates of reactions relevant to NO_3 concentration was probed. The reaction rates of NO_3 creation from $\text{NO}_2 + \text{O}_3$ (R1), thermal decomposition of N_2O_5 , and N_2O_5 formation (R2), were individually changed by their quoted error (Sander et al., 2003) for the SAGE III runs described in the model description, Sect. 3.1. The sensitivity coefficients are summarized in Table 4. The greatest sensitivity of the NO_3 column to reaction rate errors was found for the NO_3 formation reaction from $\text{NO}_2 + \text{O}_3$. The root-mean-square variation for all rate changes that increase NO_3 was 27%, and 32% for changes that decrease NO_3 column. These percent changes were applied to the TMF climatology and are plotted as the pair of dotted lines in Fig. 5. The plotted range of NO_3 columns due to reaction rate errors was of similar magnitude as the range of NO_3 values calculated from the variability observed by the TMF lidar.

Diurnal variation of NO_3 over TMF

C. M. Chen et al.

Title Page

Abstract

Introduction

Conclusions

References

Tables

Figures

◀

▶

◀

▶

Back

Close

Full Screen / Esc

Printer-friendly Version

Interactive Discussion



Acknowledgements. The research described in this paper was carried out at Jet Propulsion Laboratory, California Institute of Technology. It was supported by grants from the National Aeronautics and Space Administration. The SAGE III data used in this comparison are from L2 Lunar Event Species Profiles, v3.00, available from the NASA Langley Research Center Atmospheric Sciences Data Center (<http://eosweb.larc.nasa.gov>). We thank R. Moore for assistance with the SAGE III data, T. Leblanc for the TMF lidar data, Atmospheric and Environmental Research for use of LBLRTM, and S. Wang and A. Lambert for the orthogonal linear fit program. We also thank D. Natzic for technical assistance, L. Kovalenko for assistance with the photochemical model, and H. Bösch for discussions and calculations on atmospheric scattering. Others who have made significant technical and discussion contributions include R. Lu, D. Wu, G. Mount, V. Nemtchinov, and D. Peterson.

References

- Abbas, M. M., Gunson, M. R., Newchurch, M. J., Michelsen, H. A., Salawitch, R. J., Allen, M., Abrams, M. C., Chang, A. Y., Goldman, A., Irion, F. W., Moyer, E. J., Nagaraju, R., Rinsland, C. P., Stiller, G. P., and Zander, R.: The hydrogen budget of the stratosphere inferred from ATMOS measurements of H₂O and CH₄, *Geophys. Res. Lett.*, 23, 2405–2408, 1996. 20204, 20224
- Aldener, M., Brown, S. S., Stark, H., Williams, E. J., Lerner, B. M., Kuster, W. C., Goldan, P. D., Quinn, P. K., Bates, T. S., Fehsenfeld, F. C., and Ravishankara, A. R.: Reactivity and loss mechanisms of NO₃ and N₂O₅ in a polluted marine environment: Results from in situ measurements during New England Air Quality Study 2002, *J. Geophys. Res.-Atmos.*, 111, D23S73, doi:10.1029/2006JD007252, 2006. 20196
- Aliwell, S. R. and Jones, R. L.: Measurement of atmospheric NO₃ 1. Improved removal of water vapour absorption features in the analysis for NO₃, *Geophys. Res. Lett.*, 23, 2585–2588, 1996a. 20195
- Aliwell, S. R. and Jones, R. L.: Measurement of atmospheric NO₃ 2. Diurnal variation of stratospheric NO₃ at midlatitude, *Geophys. Res. Lett.*, 23, 2589–2592, 1996b. 20195, 20207
- Aliwell, S. R. and Jones, R. L.: Measurements of tropospheric NO₃ at midlatitude, *J. Geophys. Res.-Atmos.*, 103, 5719–5727, 1998. 20195, 20201
- Allan, B. J., McFiggans, G., Plane, J. M. C., Coe, H., and McFadyen, G. G.: The nitrate radical

Diurnal variation of NO₃ over TMF

C. M. Chen et al.

Title Page

Abstract

Introduction

Conclusions

References

Tables

Figures

◀

▶

◀

▶

Back

Close

Full Screen / Esc

Printer-friendly Version

Interactive Discussion



**Diurnal variation of
NO₃ over TMF**

C. M. Chen et al.

Title Page

Abstract

Introduction

Conclusions

References

Tables

Figures

◀

▶

◀

▶

Back

Close

Full Screen / Esc

Printer-friendly Version

Interactive Discussion



in the remote marine boundary layer, *J. Geophys. Res.-Atmos.*, 105, 24191–24204, 2000. 20196

Allan, B. J., Plane, J. M. C., Coe, H., and Shillito, J.: Observations of NO₃ concentration profiles in the troposphere, *J. Geophys. Res.-Atmos.*, 107, 4588, doi:10.1029/2002JD002112, 2002. 20195, 20196, 20211

Ambrose, J. L., Mao, H., Mayne, H. R., Stutz, J., Talbot, R., and Sive, B. C.: Nighttime nitrate radical chemistry at Appledore island, Maine during the 2004 international consortium for atmospheric research on transport and transformation, *J. Geophys. Res.-Atmos.*, 112, D21302, doi:10.1029/2007JD008756, 2007. 20196

Amekudzi, L. K., Sinnhuber, B. M., Sheode, N. V., Meyer, J., Rozanov, A., Lamsal, L. N., Bovensmann, H., and Burrows, J. P.: Retrieval of stratospheric NO₃ vertical profiles from SCIAMACHY lunar occultation measurement over the Antarctic, *J. Geophys. Res.-Atmos.*, 110, D20304, doi:10.1029/2004JD005748, 2005. 20195

Atkinson, R.: Kinetics and mechanisms of the gas-phase reactions of the NO₃ radical with organic-compounds, *J. Phys. Chem. Ref. Data*, 20, 459–507, 1991. 20195

Ayers, J. D. and Simpson, W. R.: Measurements of N₂O₅ near Fairbanks, Alaska, *J. Geophys. Res.-Atmos.*, 111, D14309, doi:10.1029/2006JD007070, 2006. 20196

Barnett, J. J. and Corney, M.: Middle atmosphere reference model derived from satellite data, Middle Atmosphere Program: Handbook for MAP Volume 16, SCOSTEP Secretariat, Univ of Illinois, Urbana, 1985. 20204, 20224

Bey, I., Jacob, D. J., Yantosca, R. M., Logan, J. A., Field, B. D., Fiore, A. M., Li, Q. B., Liu, H. G. Y., Mickley, L. J., and Schultz, M. G.: Global modeling of tropospheric chemistry with assimilated meteorology: model description and evaluation, *J. Geophys. Res.-Atmos.*, 106, 23073–23095, 2001. 20204

Brown, S. S., Dibb, J. E., Stark, H., Aldener, M., Vozella, M., Whitlow, S., Williams, E. J., Lerner, B. M., Jakoubek, R., Middlebrook, A. M., DeGouw, J. A., Warneke, C., Goldan, P. D., Kuster, W. C., Angevine, W. M., Sueper, D. T., Quinn, P. K., Bates, T. S., Meagher, J. F., Fehsenfeld, F. C., and Ravishankara, A. R.: Nighttime removal of NO_x in the summer marine boundary layer, *Geophys. Res. Lett.*, 31, L07108, doi:10.1029/2004GL019412, 2004. 20196

Brown, S. S., Dube, W. P., Osthoff, H. D., Stutz, J., Ryerson, T. B., Wollny, A. G., Brock, C. A., Warneke, C., De Gouw, J. A., Atlas, E., Neuman, J. A., Holloway, J. S., Lerner, B. M., Williams, E. J., Kuster, W. C., Goldan, P. D., Angevine, W. M., Trainer, M., Fehsenfeld, F. C., and Ravishankara, A. R.: Vertical profiles in NO₃ and N₂O₅ measured from an aircraft: Re-

**Diurnal variation of
NO₃ over TMF**

C. M. Chen et al.

[Title Page](#)[Abstract](#)[Introduction](#)[Conclusions](#)[References](#)[Tables](#)[Figures](#)[◀](#)[▶](#)[◀](#)[▶](#)[Back](#)[Close](#)[Full Screen / Esc](#)[Printer-friendly Version](#)[Interactive Discussion](#)

sults from the NOAA P-3 and surface platforms during the New England Air Quality Study 2004, *J. Geophys. Res.-Atmos.*, 112, D22304, doi:10.1029/2007JD008883, 2007a. 20196, 20211

Brown, S. S., Dubé, W. P., Osthoff, H. D., Wolfe, D. E., Angevine, W. M., and Ravishankara, A. R.: High resolution vertical distributions of NO₃ and N₂O₅ through the nocturnal boundary layer, *Atmos. Chem. Phys.*, 7, 139–149, doi:10.5194/acp-7-139-2007, 2007b. 20196

Brown, S. S., Stark, H., Ryerson, T. B., Williams, E. J., Nicks, D. K., Trainer, M., Fehsenfeld, F. C., and Ravishankara, A. R.: Nitrogen oxides in the nocturnal boundary layer: simultaneous in situ measurements of NO₃, N₂O₅, NO₂, NO, and O₃, *J. Geophys. Res.-Atmos.*, 108, 4299, doi:10.1029/2002JD002917, 2003. 20196

Cageao, R. P., Blavier, J.-F., McGuire, J. P., Jiang, Y., Nemtchinov, V., Mills, F. P., and Sander, S. P.: High-resolution Fourier-transform ultraviolet-visible spectrometer for the measurement of atmospheric trace species: application to OH, *Appl. Optics*, 40, 2024–2030, 2001. 20197

California Air Resources Board: 2007 Air Quality Data DVD, 2007. 20208

Cantrell, C. A., Davidson, J. A., Shetter, R. E., Anderson, B. A., and Calvert, J. G.: The temperature invariance of the NO₃ absorption cross-section in the 662-nm region, *J. Phys. Chem.*, 91, 5858–5863, 1987. 20198, 20200

Carlsaw, N., Carpenter, L. J., Plane, J. M. C., Allan, B. J., Burgess, R. A., Clemitshaw, K. C., Coe, H., and Penkett, S. A.: Simultaneous observations of nitrate and peroxy radicals in the marine boundary layer, *J. Geophys. Res.-Atmos.*, 102, 18917–18933, 1997a. 20196

Carlsaw, N., Plane, J. M. C., Coe, H., and Cuevas, E.: Observations of the nitrate radical in the free troposphere at Izana de Tenerife, *J. Geophys. Res.-Atmos.*, 102, 10613–10622, 1997b. 20196

Coe, H., Allan, B. J., and Plane, J. M. C.: Retrieval of vertical profiles of NO₃ from zenith sky measurements using an optimal estimation method, *J. Geophys. Res.-Atmos.*, 107, 4587–4600, 2002. 20195, 20196

Dessler, A. E., Weinstock, E. M., Hints, E. J., Anderson, J. G., Webster, C. R., May, R. D., Elkins, J. W., and Dutton, G. S.: An examination of the total hydrogen budget of the lower stratosphere, *Geophys. Res. Lett.*, 21, 2563–2566, 1994. 20204, 20224

Dütsch, H. U.: Ozone distribution in atmosphere, *Can. J. Chem.*, 52, 1491–1504, 1974. 20204, 20224

Geyer, A., Alicke, B., Ackermann, R., Martinez, M., Harder, H., Brune, W., di Carlo, P.,

**Diurnal variation of
NO₃ over TMF**

C. M. Chen et al.

Title Page

Abstract

Introduction

Conclusions

References

Tables

Figures

◀

▶

◀

▶

Back

Close

Full Screen / Esc

Printer-friendly Version

Interactive Discussion



Williams, E., Jobson, T., Hall, S., Shetter, R., and Stutz, J.: Direct observations of daytime NO₃: implications for urban boundary layer chemistry, *J. Geophys. Res.-Atmos.*, 108, 4368, doi:10.1029/2002JD002967, 2003. 20195

Geyer, A., Alicke, B., Konrad, S., Schmitz, T., Stutz, J., and Platt, U.: Chemistry and oxidation capacity of the nitrate radical in the continental boundary layer near Berlin, *J. Geophys. Res.-Atmos.*, 106, 8013–8025, 2001. 20196

Geyer, A., Alicke, B., Mihelcic, D., Stutz, J., and Platt, U.: Comparison of tropospheric NO₃ radical measurements by differential optical absorption spectroscopy and matrix isolation electron spin resonance, *J. Geophys. Res.-Atmos.*, 104, 26097–26105, 1999. 20202

Geyer, A. and Platt, U.: Temperature dependence of the NO₃ loss frequency: a new indicator for the contribution of NO₃ to the oxidation of monoterpenes and NO_x removal in the atmosphere, *J. Geophys. Res.-Atmos.*, 107, 4431, doi:10.1029/2001JD001215, 2002. 20196

Hapke, B. W., Nelson, R. M., and Smythe, W. D.: The opposition effect of the moon – the contribution of coherent backscatter, *Science*, 260, 509–511, 1993. 20197

Hauchecorne, A., Bertaux, J. L., Dalaudier, F., Cot, C., Lebrun, J. C., Bekki, S., Marchand, M., Kyrola, E., Tamminen, J., Sofieva, V., Fussen, D., Vanhellefont, F., d’Andon, O. F., Barrot, G., Mangin, A., Theodore, B., Guirlet, M., Snoeij, P., Koopman, R., de Miguel, L. S., Fraisse, R., and Renard, J. B.: First simultaneous global measurements of nighttime stratospheric NO₂ and NO₃ observed by Global Ozone Monitoring by Occultation of Stars (GOMOS)/Envisat in 2003, *J. Geophys. Res.-Atmos.*, 110, D18301, doi:10.1029/2004JD005711, 2005. 20195

Kalnay, E., Kanamitsu, M., Kistler, R., Collins, W., Deaven, D., Gandin, L., Iredell, M., Saha, S., White, G., Woollen, J., Zhu, Y., Chelliah, M., Ebisuzaki, W., Higgins, W., Janowiak, J., Mo, K. C., Ropelewski, C., Wang, J., Leetmaa, A., Reynolds, R., Jenne, R., Joseph, D.: The NCEP/NCAR 40-yr reanalysis project, *B. Am. Meteorol. Soc.*, 77, 437–471, 1996. 20212

Keating, G. M. and Young, D. F.: Interim reference ozone models for the middle atmosphere, Middle Atmosphere Program: Handbook for MAP Volume 16, SCOSTEP Secretariat, University of Illinois, Urbana, 1985. 20204, 20224

Lal, M., Sidhu, J. S., Das, S. R., and Chakrabarty, D. K.: Atmospheric NO₃ observations over low-latitude northern-hemisphere during night, *J. Geophys. Res.-Atmos.*, 98, 23029–23037, 1993. 20195

Leblanc, T.: Ozone and temperature lidar measurements obtained at Table Mountain Facility, unpublished data, California, 2005. 20203, 20231

Leblanc, T. and McDermid, I. S.: Stratospheric ozone climatology from lidar measurements at

**Diurnal variation of
NO₃ over TMF**

C. M. Chen et al.

[Title Page](#)[Abstract](#)[Introduction](#)[Conclusions](#)[References](#)[Tables](#)[Figures](#)[◀](#)[▶](#)[◀](#)[▶](#)[Back](#)[Close](#)[Full Screen / Esc](#)[Printer-friendly Version](#)[Interactive Discussion](#)

Table Mountain (34.4° N, 117.7° W) and Mauna Loa (19.5° N, 155.6° W), *J. Geophys. Res.-Atmos.*, 105, 14613–14623, 2000. 20203, 20231, 20232

Leblanc, T., McDermid, I. S., Keckhut, P., Hauchecorne, A., She, C. Y., and Krueger, D. A.: Temperature climatology of the middle atmosphere from long-term lidar measurements at middle and low latitudes, *J. Geophys. Res.-Atmos.*, 103, 17191–17204, 1998. 20203, 20231, 20232

Li, S. W., Liu, W. Q., Xie, P. N., Li, A., Qin, M., Peng, F. M., and Zhu, Y. W.: Observation of the nighttime nitrate radical in Hefei, China, *J. Environ. Sci.-China*, 20, 45–49, 2008. 20196

Lu, R. and Turco, R. P.: Air pollutant transport in a coastal environment, 2. 3-dimensional simulations over Los-Angeles Basin, *Atmos. Environ.*, 29, 1499–1518, 1995. 20206

Lu, R. and Turco, R. P.: Ozone distributions over the Los Angeles basin: three-dimensional simulations with the SMOG model, *Atmos. Environ.*, 30, 4155–4176, 1996. 20206

Lu, R., Turco, R. P., Stolzenbach, K., Friedlander, S. K., Xiong, C., Schiff, K., Tiefenthaler, L., and Wang, G. Y.: Dry deposition of airborne trace metals on the Los Angeles Basin and adjacent coastal waters, *J. Geophys. Res.-Atmos.*, 108, 4074, doi:10.1029/2001JD001446, 2003. 20206

Marchand, M., Bekki, S., Hauchecorne, A., and Bertaux, J. L.: Validation of the self-consistency of GOMOS NO₃, NO₂ and O₃ data using chemical data assimilation, *Geophys. Res. Lett.*, 31, L10107, doi:10.1029/2004GL019631, 2004. 20195

Matsumoto, J., Imagawa, K., Imai, H., Kosugi, N., Ideguchi, M., Kato, S., and Kajii, Y.: Nocturnal sink of NO_x via NO₃ and N₂O₅ in the outflow from a source area in Japan, *Atmos. Environ.*, 40, 6294–6302, 2006. 20196

Mihelcic, D., Klemp, D., Musgen, P., Patz, H. W., and Volzthomas, A.: Simultaneous measurements of peroxy and nitrate radicals at Schauinsland, *J. Atmos. Chem.*, 16, 313–335, 1993. 20196

Nakayama, T., Ide, T., Taketani, F., Kawai, M., Takahashi, K., and Matsumi, Y.: Nighttime measurements of ambient N₂O₅, NO₂, NO and O₃ in a sub-urban area, Toyokawa, Japan, *Atmos. Environ.*, 42, 1995–2006, 2008. 20196

Noxon, J. F., Norton, R. B., and Henderson, W. R.: Observation of atmospheric NO₃, *Geophys. Res. Lett.*, 5, 675–678, 1978. 20195

Noxon, J. F., Norton, R. B., and Henderson, W. R.: Comment on the problem of nighttime stratospheric NO₃ by Herman, J. R., *J. Geophys. Res.-Oc. Atm.*, 85, 4556–4557, 1980. 20195

**Diurnal variation of
NO₃ over TMF**

C. M. Chen et al.

Title Page

Abstract

Introduction

Conclusions

References

Tables

Figures

◀

▶

◀

▶

Back

Close

Full Screen / Esc

Printer-friendly Version

Interactive Discussion



- Osterman, G. B., Salawitch, R. J., Sen, B., Toon, G. C., Stachnik, R. A., Pickett, H. M., Margitan, J. J., Blavier, J. F., and Peterson, D. B.: Balloon-borne measurements of stratospheric radicals and their precursors: implications for the production and loss of ozone, *Geophys. Res. Lett.*, 24, 1107–1110, 1997. 20202
- 5 Park, R. J., Jacob, D. J., Field, B. D., Yantosca, R. M., and Chin, M.: Natural and transboundary pollution influences on sulfate-nitrate-ammonium aerosols in the United States: implications for policy, *J. Geophys. Res.-Atmos.*, 109, D15204, doi:10.1029/2003JD004473, 2004. 20204
- Platt, U., Perner, D., Winer, A. M., Harris, G. W., and Pitts, J. N.: Detection of NO₃ in the polluted troposphere by differential optical-absorption, *Geophys. Res. Lett.*, 7, 89–92, 1980. 20195
- 10 Platt, U. and Stutz, J.: *Differential Optical Absorption Spectroscopy: Principles and Applications*, Springer, Berlin Heidelberg, 2008. 20199
- Popp, P. J., Northway, M. J., Holecek, J. C., Gao, R. S., Fahey, D. W., Elkins, J. W., Hurst, D. F., Romashkin, P. A., Toon, G. C., Sen, B., Schauffler, S. M., Salawitch, R. J., Webster, C. R., Herman, R. L., Jost, H., Bui, T. P., Newman, P. A., and Lait, L. R.: Severe and extensive
- 15 denitrification in the 1999–2000 Arctic winter stratosphere, *Geophys. Res. Lett.*, 28, 2875–2878, 2001. 20224
- Ramsay, D. A.: Optical spectra of gaseous free radicals, in: *Xth Colloquium Spectroscopium Internationale, Proceedings*, edited by: Lippincott, E. R. and Margoshes, M., Spartan Books, Washington, DC, 1963. 20198
- 20 Randel, W. J., Wu, F., Russell, J. M., Waters, J.: Space-time patterns of trends in stratospheric constituents derived from UARS measurements, *J. Geophys. Res.-Atmos.*, 104, 3711–3727, 1999. 20204, 20224
- Ravishankara, A. R. and Mauldin, R. L.: Temperature-dependence of the NO₃ cross-section in the 662-nm region, *J. Geophys. Res.-Atmos.*, 91, 8709–8712, 1986. 20198, 20200, 20201
- 25 Ravishankara, A. R. and Wine, P. H.: Absorption cross-sections for NO₃ between 565 and 673 nm, *Chem. Phys. Lett.*, 101, 73–78, 1983. 20200
- Remedios, J. J., Leigh, R. J., Waterfall, A. M., Moore, D. P., Sembhi, H., Parkes, I., Greenhough, J., Chipperfield, M.P., and Hauglustaine, D.: MIPAS reference atmospheres and comparisons to V4.61/V4.62 MIPAS level 2 geophysical data sets, *Atmos. Chem. Phys. Discuss.*, 7, 9973–10017, doi:10.5194/acpd-7-9973-2007, 2007. 20204, 20224
- 30 Renard, J. B., Taupin, F. G., Riviere, E. D., Pirre, M., Huret, N., Berthet, G., Robert, C., Chartier, M., Pepe, F., and George, M.: Measurements and simulation of stratospheric NO₃ at mid and high latitudes in the Northern Hemisphere, *J. Geophys. Res.-Atmos.*, 106, 32387–

**Diurnal variation of
NO₃ over TMF**

C. M. Chen et al.

Title Page

Abstract

Introduction

Conclusions

References

Tables

Figures

◀

▶

◀

▶

Back

Close

Full Screen / Esc

Printer-friendly Version

Interactive Discussion



32399, 2001. 20195

Rinsland, C. P., Salawitch, R. J., Gunson, M. R., Solomon, S., Zander, R., Mahieu, E., Goldman, A., Newchurch, M. J., Irion, F. W., and Chang, A. Y.: Polar stratospheric descent of NO_y and CO and Arctic denitrification during winter 1992–1993, *J. Geophys. Res.-Atmos.*, 104, 1847–1861, 1999. 20224

Röckmann, T., Rhee, T. S., and Engel, A.: Heavy hydrogen in the stratosphere, *Atmos. Chem. Phys.*, 3, 2015–2023, doi:10.5194/acp-3-2015-2003, 2003. 20204, 20224

SAGE III Algorithm Theoretical Basis Document: Transmission Level 1B Products, LaRC 475-00-108 v2.1, 26 Mar 2002. 20212

Salby, M. L.: Survey of planetary-scale traveling waves – the state of theory and observations, *Rev. Geophys.*, 22, 209–236, 1984. 20206

Sander, S. P.: Temperature-dependence of the NO₃ absorption-spectrum, *J. Phys. Chem.*, 90, 4135–4142, 1986. 20198, 20200

Sander, S. P., Finlayson-Pitts, B. J., Friedl, R. R., Golden, D. M., Huie, R. E., Keller-Rudek, H., Kolb, C. E., Kurylo, M. J., Molina, M. J., Moortgat, G. K., Orkin, V. L., Ravishankara, A. R., and Wine, P. H.: Chemical Kinetics and Photochemical Data for Use in Atmospheric Studies, Evaluation Number 15, JPL Publication 06-2, Jet Propulsion Laboratory, Pasadena, 2006. 20202

Sander, S. P., Friedl, R. R., Golden, D. M., Kurylo, M. J., Huie, R. E., Orkin, V. L., Moortgat, G. K., Ravishankara, A. R., Kolb, C. E., Molina, M. J., and Finlayson-Pitts, B. J.: Chemical Kinetics and Photochemical Data for Use in Atmospheric Studies, Evaluation Number 14, JPL Publication 02-25, Jet Propulsion Laboratory, Pasadena, 2003. 20202, 20214, 20227

Sen, B., Toon, G. C., Osterman, G. B., Blavier, J. F., Margitan, J. J., Salawitch, R. J., Yue, G. K.: Measurements of reactive nitrogen in the stratosphere, *J. Geophys. Res.-Atmos.*, 103, 3571–3585, 1998. 20204, 20224

Smith, J. P. and Solomon, S.: Atmospheric NO₃ 3. Sunrise disappearance and the stratospheric profile, *J. Geophys. Res.-Atmos.*, 95, 13819–13827, 1990. 20195

Smith, J. P., Solomon, S., Sanders, R. W., Miller, H. L., Perliski, L. M., Keys, J. G., and Schmeltekopf, A. L.: Atmospheric NO₃ 4. Vertical profiles at middle and polar latitudes at sunrise, *J. Geophys. Res.-Atmos.*, 98, 8983–8989, 1993. 20195

Smith, N., Plane, J. M. C., Nien, C. F., and Solomon, P. A.: Nighttime radical chemistry in the San-Joaquin Valley, *Atmos. Environ.*, 29, 2887–2897, 1995. 20196

Solomon, S., Miller, H. L., Smith, J. P., Sanders, R. W., Mount, G. H., Schmeltekopf, A. L., and

**Diurnal variation of
NO₃ over TMF**

C. M. Chen et al.

Title Page

Abstract

Introduction

Conclusions

References

Tables

Figures

◀

▶

◀

▶

Back

Close

Full Screen / Esc

Printer-friendly Version

Interactive Discussion



Noxon, J. F.: Atmospheric NO₃ 1. Measurement technique and the annual cycle at 40° N, J. Geophys. Res.-Atmos., 94, 11041–11048, 1989. 20195, 20201, 20207

Stutz, J., Alicke, B., Ackermann, R., Geyer, A., White, A., and Williams, E.: Vertical profiles of NO₃, N₂O₅, O₃, and NO_x in the nocturnal boundary layer: 1. Observations during the Texas Air Quality Study 2000, J. Geophys. Res.-Atmos., 109, D12306, doi:10.1029/2003JD004209, 2004. 20196

Stutz, J. and Platt, U.: Numerical analysis and estimation of the statistical error of differential optical absorption spectroscopy measurements with least-squares methods, Appl. Optics, 35, 6041–6053, 1996. 20199

Toon, G. C.: The JPL MkIV interferometer, Opt. Photonics News, 2, 19–21, 1991. 20204, 20224

Thomason, L. W., Poole, L. R., and Deshler, T.: A global climatology of stratospheric aerosol surface area density deduced from stratospheric aerosol and gas experiment II measurements: 1984–1994, J. Geophys. Res.-Atmos., 102, 8967–8976, 1997. 20204, 20224

von Friedeburg, C., Wagner, T., Geyer, A., Kaiser, N., Vogel, B., Vogel, H., and Platt, U.: Derivation of tropospheric NO₃ profiles using off-axis differential optical absorption spectroscopy measurements during sunrise and comparison with simulations, J. Geophys. Res.-Atmos., 107, 4168, doi:10.1029/2001JD000481, 2002. 20195, 20196

Vrekoussis, M., Mihalopoulos, N., Gerasopoulos, E., Kanakidou, M., Crutzen, P. J., and Lelieveld, J.: Two-years of NO₃ radical observations in the boundary layer over the Eastern Mediterranean, Atmos. Chem. Phys., 7, 315–327, doi:10.5194/acp-7-315-2007, 2007. 20196

Wamsley, P. R., Elkins, J. W., Fahey, D. W., Dutton, G. S., Volk, C. M., Myers, R. C., Montzka, S. A., Butler, J. H., Clarke, A. D., Fraser, P. J., Steele, L. P., Lucarelli, M. P., Atlas, E. L., Schauffler, S. M., Blake, D. R., Rowland, F. S., Sturges, W. T., Lee, J. M., Penkett, S. A., Engel, A., Stimpfle, R. M., Chan, K. R., Weisenstein, D. K., Ko, M. K. W., and Salawitch, R. J.: Distribution of halon-1211 in the upper troposphere and lower stratosphere and the 1994 total bromine budget, J. Geophys. Res.-Atmos., 103, 1513–1526, 1998. 20224

Wang, H. J., Cunnold, D. M., Froidevaux, L., and Russell, J. M.: A reference model for middle atmosphere ozone in 1992–1993, J. Geophys. Res.-Atmos., 104, 21629–21643, 1999. 20204, 20224

Wang, S., Ackermann, R., and Stutz, J.: Vertical profiles of O₃ and NO_x chemistry in the polluted nocturnal boundary layer in Phoenix, AZ: I. Field observations by long-path DOAS, Atmos. Chem. Phys., 6, 2671–2693, doi:10.5194/acp-6-2671-2006, 2006. 20196

**Diurnal variation of
NO₃ over TMF**

C. M. Chen et al.

[Title Page](#)[Abstract](#)[Introduction](#)[Conclusions](#)[References](#)[Tables](#)[Figures](#)[◀](#)[▶](#)[◀](#)[▶](#)[Back](#)[Close](#)[Full Screen / Esc](#)[Printer-friendly Version](#)[Interactive Discussion](#)

Wang, S. H., Pickett, H. M., Pongetti, T. J., Cheung, R., Yung, Y. L., Shim, C., Li, Q. B., Canty, T.,
Salawitch, R. J., Jucks, K. W., Drouin, B., and Sander, S. P.: Validation of aura microwave limb
sounder OH measurements with Fourier transform ultra-violet spectrometer total OH col-
umn measurements at Table Mountain, California, *J. Geophys. Res.-Atmos.*, 113, D22301,
doi:10.1029/2008JD009883, 2008. 20213

Wayne, R. P., Barnes, I., Biggs, P., Burrows, J. P., Canosamas, C. E., Hjorth, J., Lebras, G.,
Moortgat, G. K., Perner, D., Poulet, G., Restelli, G., and Sidebottom, H.: The nitrate radical
– physics, chemistry, and the atmosphere, *Atmos. Environ. A-Gen.*, 25, 1–203, 1991. 20195

Weaver, A., Solomon, S., Sanders, R. W., Arpag, K., and Miller, H. L.: Atmospheric NO₃. 5.
Off-axis measurements at sunrise: estimates of tropospheric NO₃ at 40°N, *J. Geophys.*
Res.-Atmos., 101, 18605–18612, 1996. 20195

Wu, D. L. and Waters, J. W.: Satellite observations of atmospheric variances: A possible indi-
cation of gravity waves, *Geophys. Res. Lett.*, 23, 3631–3634, 1996. 20206

Wu, S. L., Mickley, L. J., Jacob, D. J., Logan, J. A., Yantosca, R. M., and Rind, D.: Why are there
large differences between models in global budgets of tropospheric ozone?, *J. Geophys.*
Res.-Atmos., 112, D05302, doi:10.1029/2006JD007801, 2007. 20204

Yang, E.-S., Cunnold, D. M., Salawitch, R. J., McCormick, M. P., Russell III, J., Zawodny, J. M.,
Oltmans, S., and Newchurch, M. J.: Attribution of recovery in lower-stratospheric ozone, *J.*
Geophys. Res., 111, D17309, doi:10.1029/2005JD006371, 2006. 20202, 20204

Yokelson, R. J., Burkholder, J. B., Fox, R. W., Talukdar, R. K., and Ravishankara, A. R.:
Temperature-dependence of the NO₃ absorption-spectrum, *J. Phys. Chem.*, 98, 13144–
13150, 1994. 20198, 20200, 20201, 20202

Table 1. Sources for the input parameters for each of the cases run on the 1-D stratospheric model.

Input parameter	Model run		
	TMF	SAGE III	sensitivity
temperature	TMF lidar data [‡]	From Sage III NO ₃ retrieval [‡]	URAP baseline dataset [‡]
O ₃	TMF lidar data [‡]	From Sage III NO ₃ retrieval [‡]	URAP extended dataset [‡]
H ₂ O	URAP, extended dataset [‡]		
CH ₄	URAP, extended dataset [‡]		
NO _y	Calculated from tracer relation (Rinsland et al., 1999; Popp et al., 2001) using URAP N ₂ O baseline dataset [‡]		
Cl _y	Calculated from tracer relation from SOLVE data, using URAP N ₂ O baseline dataset [‡]		
CO	Static profile from MkIV flight (Toon, 1991; Sen et al., 1998)		
H ₂	Static profile based on measurements (Dessler et al., 1994; Abbas et al., 1996; Rockmann et al., 2003)		
C ₂ H ₆	Static profile from MkIV flight (Toon, 1991; Sen et al., 1998)		
Br _y	Calculated from tracer relation (Wamsley et al., 1998) using URAP N ₂ O baseline dataset [‡]		
aerosol parameters	Monthly profiles from SAGE II aerosol measurements averaged over all years except those affected by the Pinatubo eruption (Thomason et al., 1997)		

[‡] Gaps filled first with URAP data (Remedios et al., 2007; Wang et al., 1999; Randel et al., 1999). For ozone, further gaps were filled by a climatology based on Dütsch (Dütsch, 1974), on the Middle Atmosphere Project (Keating and Young, 1985), and from many in situ ozone measurements in the lower stratosphere and upper troposphere. For temperature, further gaps were filled from the Middle Atmosphere Project (Barnett and Corney, 1985).

[†] URAP data is available averaged over 7 yr (extended) or over 1992–1993 (baseline).

**Diurnal variation of
NO₃ over TMF**

C. M. Chen et al.

Title Page

Abstract	Introduction
Conclusions	References
Tables	Figures
◀	▶
◀	▶
Back	Close
Full Screen / Esc	
Printer-friendly Version	
Interactive Discussion	



Diurnal variation of NO₃ over TMF

C. M. Chen et al.

Table 2. Summary of NO₃ seasonal mean columns (in molec cm⁻²) calculated for the subset of observations with “model-like behavior”, and for results from the 1-D stratospheric model using profiles from the lidar at TMF with monthly mean fields from 2003 and 2004 and ten year climatological inputs. There were no measurements during the October through March months in 2003. The standard deviation of the mean columns is shown in parentheses.

	Apr–Sep NO ₃ Mean Col (Std Dev)	Oct–Mar NO ₃ Mean Col (Std Dev)
Obs. (subset) 2003	7.5 (1.5) × 10 ¹³	–
Obs. (subset) 2004	7.5 (1.5) × 10 ¹³	5.5 (0.8) × 10 ¹³
Model (TMF 2003)	4.1 (0.5) × 10 ¹³	3.0 (0.4) × 10 ¹³
Model (TMF 2004)	3.9 (0.6) × 10 ¹³	3.3 (1.0) × 10 ¹³
Model (TMF climatology)	4.7 (0.4) × 10 ¹³	3.1 (0.5) × 10 ¹³

[Title Page](#)
[Abstract](#)
[Introduction](#)
[Conclusions](#)
[References](#)
[Tables](#)
[Figures](#)
[I◀](#)
[▶I](#)
[◀](#)
[▶](#)
[Back](#)
[Close](#)
[Full Screen / Esc](#)
[Printer-friendly Version](#)
[Interactive Discussion](#)


Diurnal variation of NO₃ over TMF

C. M. Chen et al.

Table 3. Mean, median, and standard deviation of column NO₃ from the GEOS-Chem 3-D global transport and chemistry model for the evenings of 28–30 August 2004 and 27–29 September 2004, which coincide with data collection days. Four regions were investigated, Los Angeles (contains TMF), Northern Midlatitude Pacific, Western Colorado, and the northern midlatitude band (30–45° N). The columns are calculated as total, the column below the maximum extent of the boundary layer for the previous day, and the column above.

	NO ₃ Mean Column ($\times 10^{13}$ cm ⁻²)					
	Los Angeles			N Midlat Pacific		
	Total	BL*	FT*	Total	BL*	FT*
28 Aug 04	71	73	13	5.6	0.018	5.6
29 Aug 04	69	59	10	5.3	0.015	5.3
30 Aug 04	73	64	9.3	5.2	0.015	5.2
27 Sep 04	54	48	5.5	4.7	0.033	4.7
28 Sep 04	34	28	5.4	5.0	0.051	5.0
29 Sep 04	16	10	5.7	5.0	0.097	4.9
	Western Colorado			Northern midlatitude band		
	Total	BL*	FT*	Total	BL*	FT*
	Total	BL*	FT*	Total	BL*	FT*
28 Aug 04	4.3	3.3	1.1	9.6	3.3	6.4
29 Aug 04	5.7	4.7	1.0	9.0	2.9	6.1
30 Aug 04	7.0	6.0	0.95	8.9	2.9	6.0
27 Sep 04	4.5	3.5	1.1	9.7	3.8	5.8
28 Sep 04	4.5	2.4	2.1	9.4	3.4	6.0
29 Sep 04	2.9	1.9	0.98	11	3.8	6.8

[Title Page](#)
[Abstract](#)
[Introduction](#)
[Conclusions](#)
[References](#)
[Tables](#)
[Figures](#)
[I◀](#)
[▶I](#)
[◀](#)
[▶](#)
[Back](#)
[Close](#)
[Full Screen / Esc](#)
[Printer-friendly Version](#)
[Interactive Discussion](#)


Diurnal variation of NO₃ over TMF

C. M. Chen et al.

Title Page

Abstract

Introduction

Conclusions

References

Tables

Figures

◀

▶

◀

▶

Back

Close

Full Screen / Esc

Printer-friendly Version

Interactive Discussion



Table 4. Summary of sensitivity coefficients due to variations in temperature, ozone, and relevant reaction rate constants. Temperature was varied by ± 5 K, ozone by $\pm 5\%$, NO_y by $\pm 5\%$, and the rate constants were varied by their quoted error limits (Sander et al., 2003).

	Sensitivity coefficients	
	Negative variation	Positive variation
Temperature (5 K)	-0.25	0.36
O ₃ (5%)	-0.05	0.05
NO _y (5%)	-0.01	0.01
NO ₂ + O ₃ → NO ₃ + O ₂	-0.24	0.29
N ₂ O ₅ → NO ₃ + NO ₂	-0.04	0.06
NO ₃ + NO ₂ + M ↔ N ₂ O ₅ + M	0.12	-0.12

Diurnal variation of NO_3 over TMF

C. M. Chen et al.

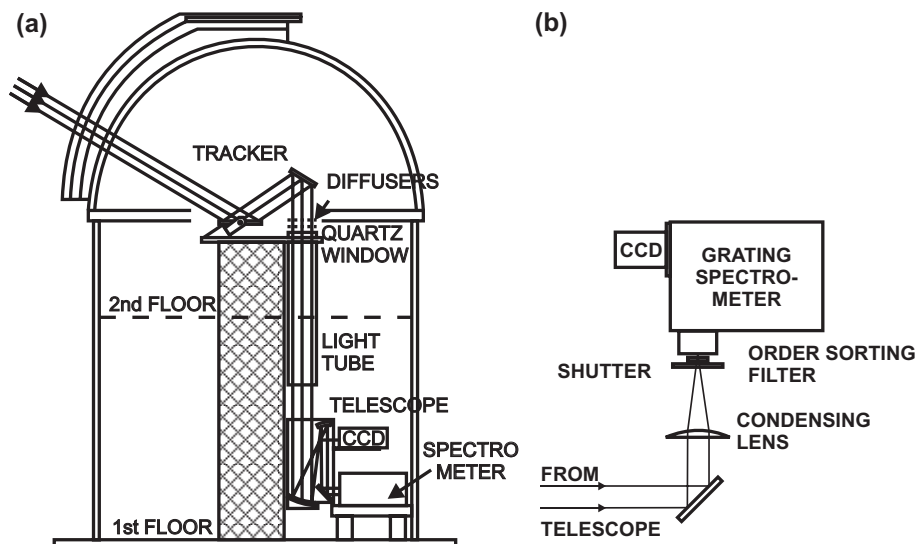


Fig. 1. Schematic of the instrument light path. **(a)** Light is collected by the primary of the heliostat (tracker), reflected down to the telescope on the first floor which conditions it to a 7 cm diameter collimated beam. **(b)** The light is then reflected to a condensing lens, past a shutter, order-sorting filter, and then into the spectrometer, recorded by a CCD.

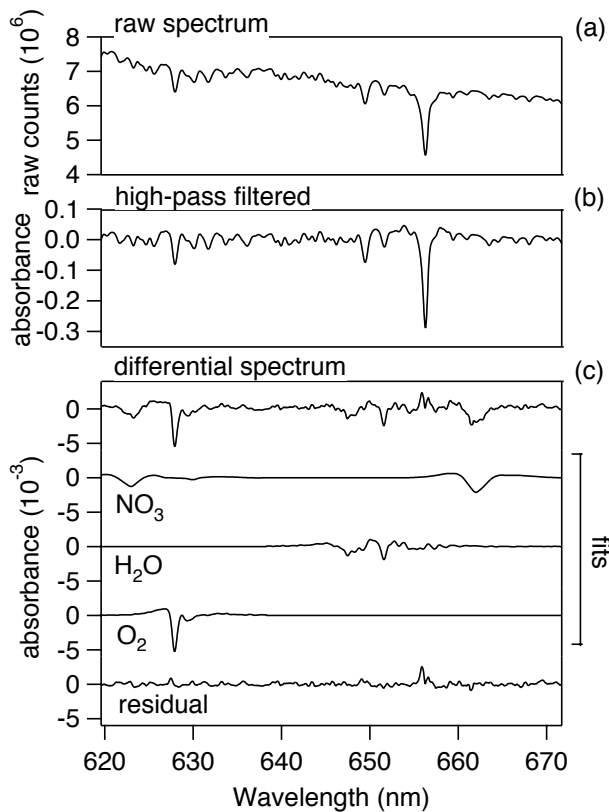


Fig. 2. Spectra at different stages of processing: **(a)** raw spectrum, with visibly sloping baseline, **(b)** high-pass filtered raw spectrum, created by dividing the raw spectrum with a smoothed version, and **(c)** the differential spectrum, after subtracting the solar reference spectrum (similar to **(b)**), with the individual fits for NO₃, water, oxygen, and the resultant residual. The residual features result from errors in fitting the solar line.

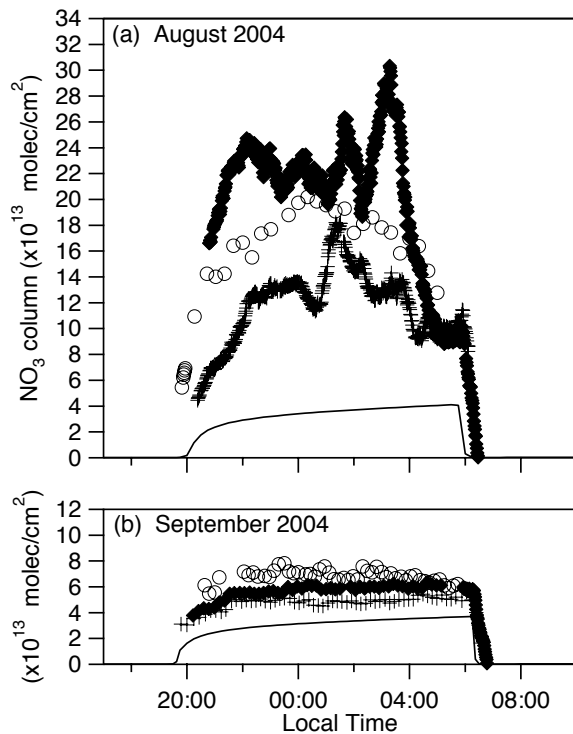


Fig. 3. Diurnal variation of NO_3 vertical column measured at Table Mountain, California for August and September 2004, along with calculated vertical columns from the 1-D stratospheric model (line). For August 2004 **(a)**, three consecutive evenings of measurements are shown, the evenings of 28 August 2004 (open circle), 29 August 2004 (+), and 30 August 2004 (filled diamond). Also for September 2004 **(b)**, three consecutive evenings of measurements are shown the evenings of 27 September 2004 (open circle), 28 September 2004 (+), and 29 September 2004 (filled diamond). The stratospheric model used monthly mean profiles from TMF lidar measurements from 2004 as input. Data from September, during the steady state nocturnal period, shows only every tenth point to avoid crowding the graph.

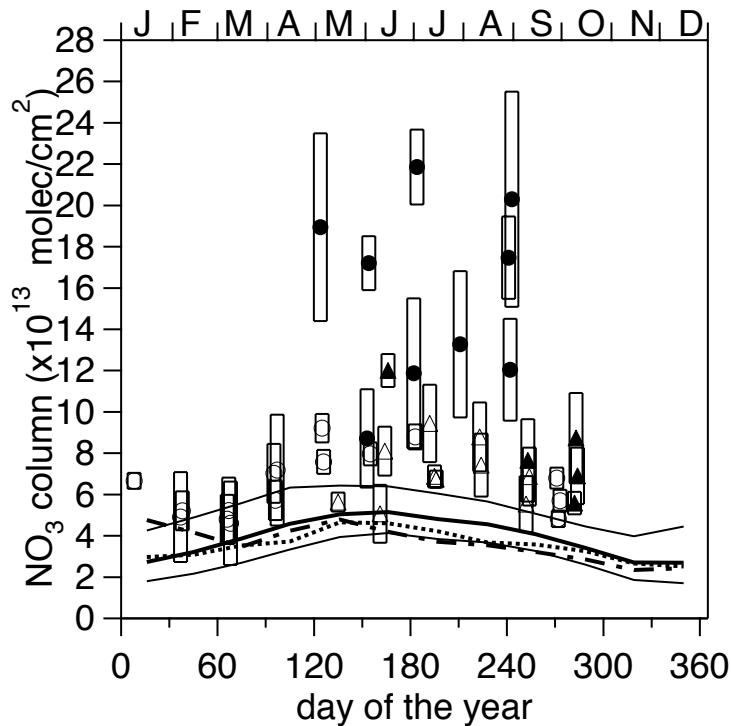


Fig. 4. Table Mountain Facility (TMF) NO_3 vertical column measurements compared to results from the 1-D photochemical model using TMF lidar profiles of ozone and temperature as inputs, plotted vs. day of year. Both the measured and modeled columns were averaged over the steady state portion of the night. The measured mean NO_3 columns shown are from 2003 (triangles)–2004 (circles); model-like and non-modeled behavior are denoted by open and filled symbols, respectively. The bars show the diurnal variability. The three cases run by the model are: the climatology from 1988–1997 along with the limits of the temperature and ozone variability taken from Leblanc et al. (1998); Leblanc and McDermid (2000), and mean profiles from Leblanc (2005) for 2003 and 2004.

Diurnal variation of NO_3 over TMF

C. M. Chen et al.

Title Page	
Abstract	Introduction
Conclusions	References
Tables	Figures
◀	▶
◀	▶
Back	Close
Full Screen / Esc	
Printer-friendly Version	
Interactive Discussion	



Diurnal variation of
NO₃ over TMF

C. M. Chen et al.

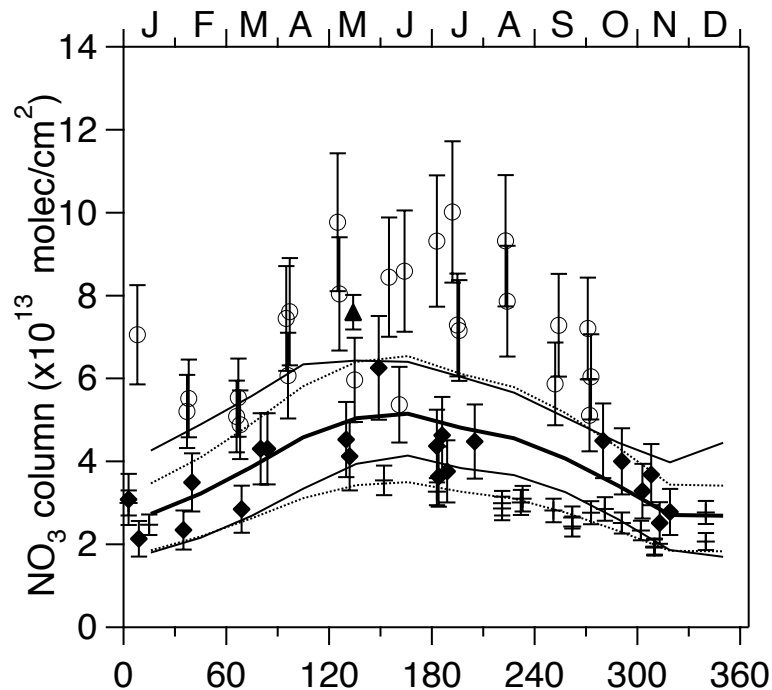


Fig. 5. Subset of the NO₃ vertical columns measured at Table Mountain Facility (TMF) that followed model-like behavior (open circle), data from Aliwell and Jones (filled triangle), Solomon et al. (filled diamond), and SAGE III satellite measurements (+) plotted versus day of year. These measurements are compared to a stratospheric photochemical 1-D model with temperature and ozone concentrations from a TMF climatology from 1988–1997 (thick line), along with the limits of the temperature and ozone variability (thin line) taken from Leblanc et al. (1998); Leblanc and McDermid (2000). The uncertainty in the NO₃ column due to the uncertainty in the rate constants for N₂O₅ thermal decomposition, and Reactions (R1) and (R2) are also shown in this figure (dotted line).

Title Page

Abstract

Introduction

Conclusions

References

Tables

Figures

◀

▶

◀

▶

Back

Close

Full Screen / Esc

Printer-friendly Version

Interactive Discussion



**Diurnal variation of
NO₃ over TMF**

C. M. Chen et al.

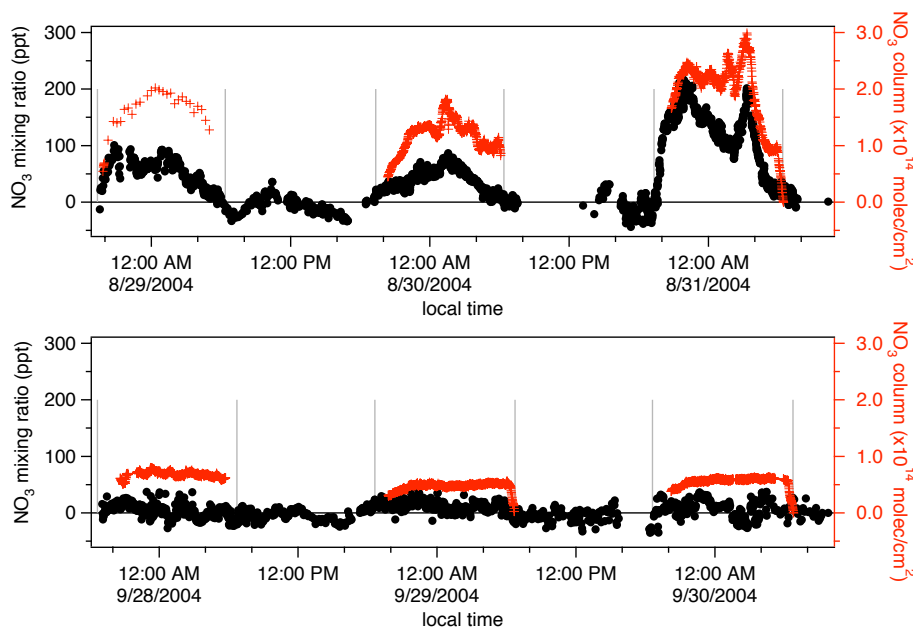


Fig. 6. Coincident measurements of NO₃ vertical column (in red) using lunar occultation and surface measurements of NO₃ concentration (in black) using long-path DOAS. Many of the large features in the data taken in August 2004 occur in both datasets. Measurements in September 2004 verify that there were very low levels of NO₃ concentration at the surface the whole evening.

[Title Page](#)[Abstract](#)[Introduction](#)[Conclusions](#)[References](#)[Tables](#)[Figures](#)[◀](#)[▶](#)[◀](#)[▶](#)[Back](#)[Close](#)[Full Screen / Esc](#)[Printer-friendly Version](#)[Interactive Discussion](#)

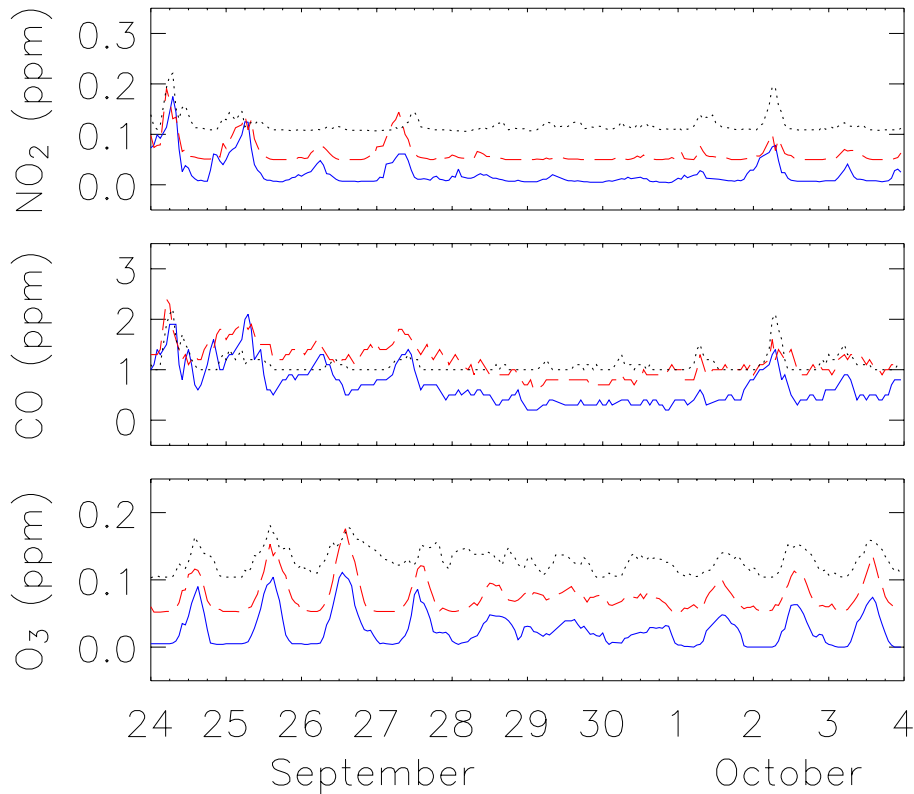


Fig. 7. Time series data for NO_2 , CO , and O_3 mixing ratio (offset progressively by 0.05 ppm) at three AQMD monitoring sites located in the Mojave Desert and progressively towards Los Angeles: Victorville (black dot), Azusa (red dash), and downtown Los Angeles (blue solid). The Santa Ana winds occurred 28–30 September 2004, evidenced by the disturbance of the diurnal cycle and lower diurnal concentrations. The date labels correspond to 00:00 LT for each day.

Diurnal variation of NO_3 over TMF

C. M. Chen et al.

Title Page	
Abstract	Introduction
Conclusions	References
Tables	Figures
◀	▶
◀	▶
Back	Close
Full Screen / Esc	
Printer-friendly Version	
Interactive Discussion	



Diurnal variation of NO_3 over TMF

C. M. Chen et al.

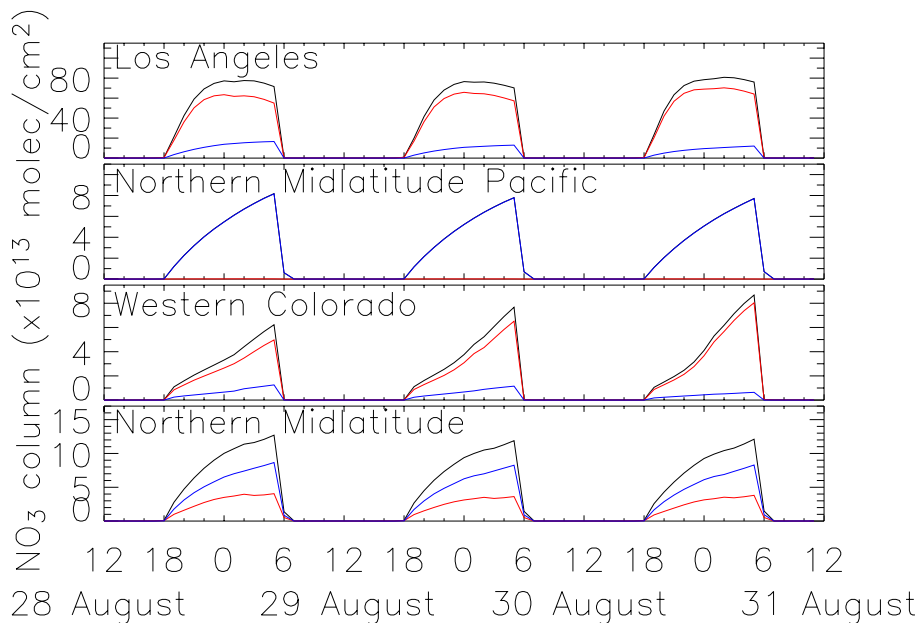


Fig. 8. Time evolution of total tropospheric vertical column (black), “maximum boundary layer” vertical column (red), and “minimum free tropospheric” vertical column (blue) as calculated from 3-D global chemical transport model GEOS-Chem, for four different regions during three days in August. The “maximum boundary layer” column for an evening is the column calculated from the surface to the height of the maximum thickness boundary layer from the preceding day. The minimum free troposphere is the difference between the total tropospheric column and the maximum boundary layer. The four regions are Los Angeles ($33\text{--}35^\circ\text{N}$, $241.25\text{--}243.75^\circ\text{E}$), Western Colorado ($37\text{--}41^\circ\text{N}$, $251.25\text{--}253.75^\circ\text{E}$), the Northern Midlatitude Pacific Ocean ($29\text{--}45^\circ\text{N}$, $178.75\text{--}228.75^\circ\text{E}$), and in the northern midlatitude band ($29\text{--}45^\circ\text{N}$).

Title Page

Abstract

Introduction

Conclusions

References

Tables

Figures

◀

▶

◀

▶

Back

Close

Full Screen / Esc

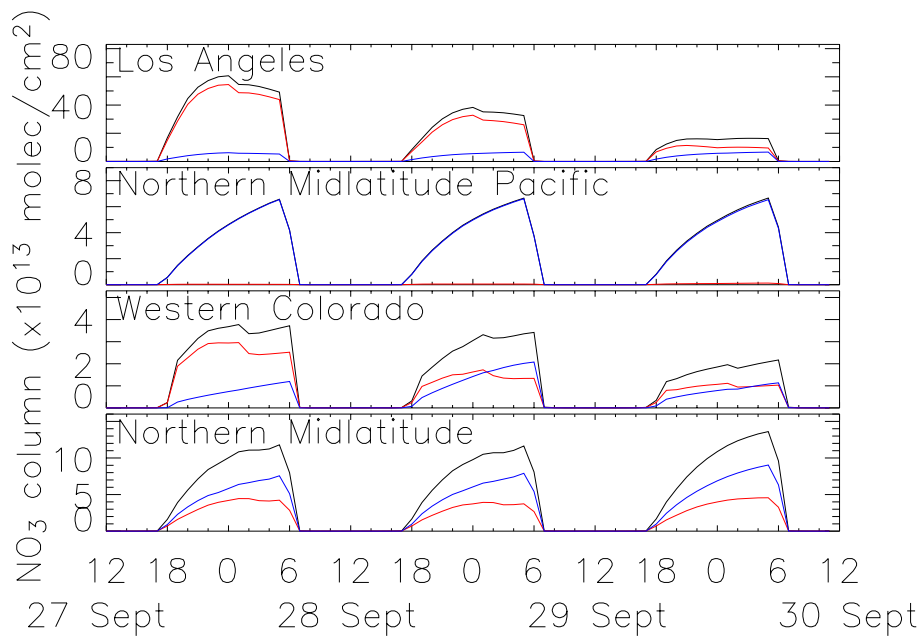
Printer-friendly Version

Interactive Discussion



**Diurnal variation of
NO₃ over TMF**

C. M. Chen et al.

**Fig. 9.** Same as Fig. 8 except for September.[Title Page](#)[Abstract](#)[Introduction](#)[Conclusions](#)[References](#)[Tables](#)[Figures](#)[◀](#)[▶](#)[◀](#)[▶](#)[Back](#)[Close](#)[Full Screen / Esc](#)[Printer-friendly Version](#)[Interactive Discussion](#)

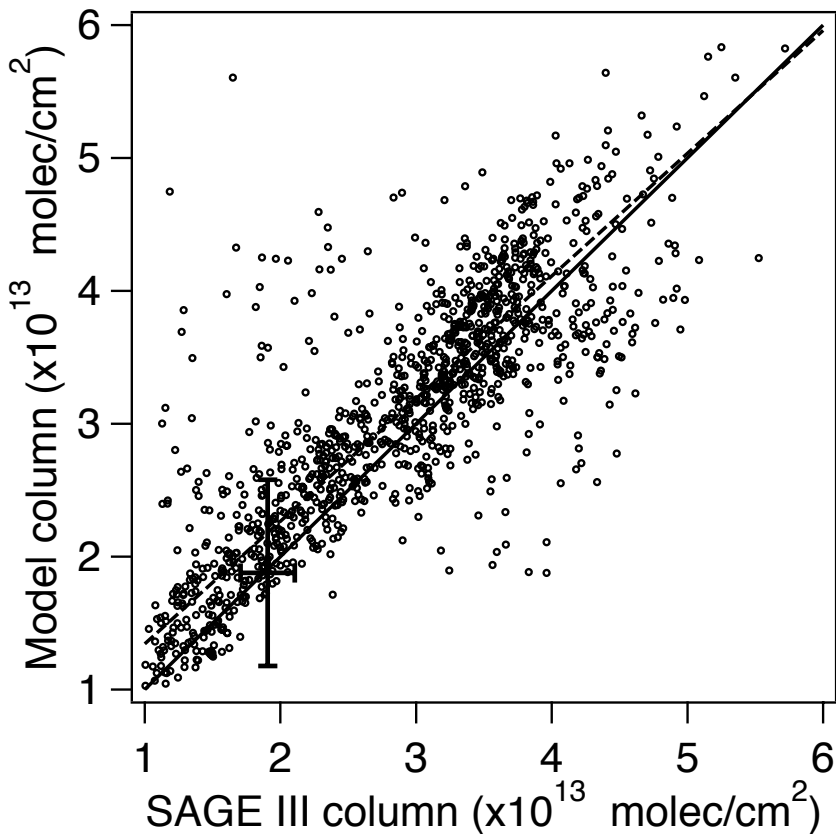


Fig. 10. Modeled NO_3 vertical columns using SAGE III lunar profiles as model input, compared to the SAGE III measured NO_3 columns within a band from 70°S to 70°N . The one-to-one line is shown as a solid line, and a linear fit to the data (with a slope of 0.92) is shown as a dashed line. The uncertainty in the SAGE III NO_3 column (2×10^{12} molec cm^{-2}) and the uncertainty in the modeled column (7×10^{12} molec cm^{-2}) are shown on one data point.

Diurnal variation of NO_3 over TMF

C. M. Chen et al.

Title Page	
Abstract	Introduction
Conclusions	References
Tables	Figures
◀	▶
◀	▶
Back	Close
Full Screen / Esc	
Printer-friendly Version	
Interactive Discussion	

